

© 2019 Yufang Yao

EVALUATION AND VISUALIZATION OF REFRIGERANT TWO-PHASE FLOW IN
DISTRIBUTOR

BY

YUFANG YAO

THESIS

Submitted in partial fulfillment of the requirements
for the degree of Master of Science in Mechanical Engineering
in the Graduate College of the
University of Illinois at Urbana-Champaign, 2019

Urbana, Illinois

Adviser:

Professor Pega S. Hrnjak

ABSTRACT

This study aims at understanding flow distribution exiting thermostatic expansion valve and through distributor. It is well known that when two-phase flow goes through separation devices such as distributors and headers, mal-distribution is unavoidable due to different properties of liquid and vapor. However, it is possible to reduce mal-distribution by better design or creating proper working conditions. In this study, several parameters that may influence the flow distribution such as mass flow rate, distributor inlet quality, and orientation are studied. Refrigerant mal-distribution is quantified by comparing mass flow rate, quality, and cooling capacity in each circuit. To make the experiment results more applicable to real system, several aspects in this facility which are not exactly the same with real air conditioning system are analyzed, including the extra pressure drop due to mass flow meter and the different design of evaporator. What's more, two-phase flow exiting thermostatic expansion valve and through distributor is visualized by high-speed camera to get a deeper understanding about what happened in this region.

It was found that better distribution can be achieved at higher mass flow rate and lower distributor inlet quality, because flow velocity increases as mass flow rate gets higher, which contributes to form more homogeneous flow. And decrease in quality makes the two-phase flow closer to single phase. Orientation was found to have no influence on distribution, since the distributor is installed quite close to the exit of thermostatic expansion valve where the phase separation does not happen. The pressure drop due to mass flow meter was proved helpful to achieve better distribution, which means the performance of distributor was a little overestimated by experiments in this study. According to the visualization, flow regime at the inlet of distributor is somewhere between annular flow and homogeneous flow with variation of mass flow rate.

ACKNOWLEDGMENTS

I would like to dedicate my most sincere gratitude to my adviser, Professor Predrag S. Hrnjak. He is kind, patient, and encouraging to all his students. His broad knowledge and deep insights inspire me a lot and guide me to go further. I also want to express my thankfulness to the generous help provided by Raghu Kunapuli, Dave Wrocklage, Tim Roberts and all other representatives from Parker Hannifin. Their financial support and valuable advices are of great help to this project. I would also like to deliver my gratitude to Li Huang and Hui Zhao in Creative Thermal Solution for their help in instrument calibrating and material polishing. I want to thank all my colleagues in ACRC group for their suggestions in various aspects. They are willing to share everything they know to others and provide generous help whenever I need.

Also, special thanks to my boyfriend Hongliang Qian. He accompanied me through every hard time and shared my happiness in life and research. At last, I want to thank my parents and my brother for their unconditional love and support. They are always comforting and giving me a shelter to rest on.

TABLE OF CONTENTS

LIST OF FIGURES	vi
LIST OF TABLES	ix
NOMENCLATURE	x
CHAPTER 1 INTRODUCTION	1
1.1 Refrigerant distributor in air conditioning system	1
1.2 Literature review	2
1.2.1 Experiment investigation	3
1.2.2 Numerical simulation.....	5
CHAPTER 2 EXPERIMENT SETUP.....	7
2.1 Facility.....	7
2.2 Experiment procedures and conditions	10
2.3 Data reduction and uncertainty	11
CHAPTER 3 EXPERIMENT RESULTS UNDER DIFFERENT WORKING CONDITIONS..	15
3.1 Effect of refrigerant mass flow rate.....	15
3.2 Effect of distributor inlet quality	19
3.3 Effect of orientation	22
CHAPTER 4 COMPARISON WITH REAL SYSTEM	25
4.1 Influence of pressure drop from Micro Motion on distribution	25
4.2 Uniform heat load vs. uniform superheat.....	30
4.3 Degradation in capacity due to maldistribution	32
CHAPTER 5 VISUALIZATION	36
5.1 Representativeness of the transparent distributor.....	36
5.2 Visualization of refrigerant two-phase flow in distributor.....	38
CHAPTER 6 CONCLUSION.....	42

6.1 Summary 42

6.2 Future work 43

REFERENCES 44

APPENDIX A PRESSURE DROP IN FEEDER TUBE..... 47

APPENDIX B CALCULATED PRESSURE DROP VS. MEASURED PRESSURE DROP 48

APPENDIX C REPRESENTATIVENESS OF THE TRANSPARENT DISTRIBUTOR..... 49

APPENDIX D ORIGINAL DATA..... 51

LIST OF FIGURES

Figure 1 Structure of the nozzle type distributor [2].....	1
Figure 2 Structure of Venturi distributor [2].....	2
Figure 3 Structure of distributor with the mechanism of separating and then distributing [3].....	2
Figure 4 Experimental facility	7
Figure 5 Schematic drawing of experimental facility.....	8
Figure 6 thermal expansion valve and distributor assembly.....	9
Figure 7 Schematic drawing of the evaporator	9
Figure 8 Transparent distributor and TEV assembly	10
Figure 9 Parameters measured in this study	13
Figure 10 Distribution of mass flow rate and quality (m=15 g/s, x=0.22, horizontal).....	15
Figure 11 Front view and side view of the distributor.....	16
Figure 12 Distribution of non-dimensional mass flow rate, quality and heat load (x=0.22, horizontal).....	17
Figure 13 Distribution of non-dimensional mass flow rate, quality and heat load (x=0.22, vertical downward)	18
Figure 14 Distribution of non-dimensional mass flow rate, quality and heat load (x=0.22, vertical upward)	19
Figure 15 Distribution of non-dimensional mass flow rate, quality and heat load (m=25 g/s, horizontal).....	20
Figure 16 Distribution of non-dimensional mass flow rate, quality and heat load (m=25 g/s, vertical downward)	21
Figure 17 Distribution of non-dimensional mass flow rate, quality and heat load (m=25 g/s, vertical upward)	22

Figure 18 Standard deviation of mass flow rate, heat load and quality as a function of total mass flow rate	24
Figure 19 Standard deviation of mass flow rate, heat load and quality as a function of distributor inlet quality	24
Figure 20 Top view of the test section in this study	25
Figure 21 Measured pressure at three different locations	26
Figure 22 Distribution of non-dimensional heat load with and without Micro Motion (x=0.22, vertical downward orientation)	27
Figure 23 Standard deviation of heat load with and without Micro Motion	27
Figure 24 Schematic of pressure drop partition for each component	28
Figure 25 Adiabatic two-phase flow pressure drop as a function of mass flow rate and quality (horizontal, m=15 g/s, x=0.22)	29
Figure 26 Pressure drop (ΔP_4) as a function of mass flow rate	30
Figure 27 Distribution of mass flow rate and superheat (vertical upwards, x=0.22)	31
Figure 28 Standard deviation of mass flow rate and quality (vertical upwards, x=0.22)	32
Figure 29 Demonstration of key parameters controlled as constant under three operating modes	33
Figure 30 Distribution of mass flow rate, quality, heat load and superheat under three operating modes (x=0.22, vertical downwards)	34
Figure 31 Capacity ratio under three operating modes	35
Figure 32 Location of circuits for original and transparent distributor	36
Figure 33 Distribution of non-dimensional heat load: original distributor vs. transparent distributor (horizontal, x=0.22)	37
Figure 34 Visualization of two-phase flow in distributor and the inlet tube (horizontal)	39
Figure 35 Velocity vector contours in distributor [16]	40
Figure 36 Visualization of two-phase flow in distributor and the inlet tube (vertical downward)	40

Figure 37 Visualization of two-phase flow in distributor and the inlet tube (vertical upward)....	41
Figure 38 Adiabatic two-phase flow pressure drop as a function of mass flow rate and quality (horizontal, $m=20$ g/s, $x=0.22$)	47
Figure 39 Adiabatic two-phase flow pressure drop as a function of mass flow rate and quality (horizontal, $m=25$ g/s, $x=0.22$)	47
Figure 40 Comparison of pressure drop between calculated and measured values.....	48
Figure 41 Distribution of non-dimensional het load: original distributor vs. transparent distributor (vertical downward, $x=0.22$).....	49
Figure 42 Distribution of non-dimensional het load: original distributor vs. transparent distributor (vertical upward, $x=0.22$).....	50

LIST OF TABLES

Table 1 Experiment conditions	10
Table 2 Parameters for method 1 to calculate mass flow rate of liquid phase refrigerant before distributor	12
Table 3 Parameters for method 2 to calculate mass flow rate of liquid phase refrigerant after distributor	13
Table 4 Uncertainties of measurement	13
Table 5 Experiment results under five working conditions at vertical upward orientation	51
Table 6 Experiment results under five working conditions at vertical downward orientation	52
Table 7 Experiment results under five working conditions at horizontal orientation	53
Table 8 Experiment results without Micro Motion under three working conditions at vertical downward orientation	54
Table 9 Experiment results with uniform heat load under three working conditions at vertical upward orientation	55
Table 10 Experiment results with uniform heat load under three working conditions at vertical downward orientation	56
Table 11 Experiment results with uniform mass flow rate under three working conditions at vertical downward orientation	57

NOMENCLATURE

C	Maximum cooling capacity difference	-
D	Distributor diameter	mm
h	Refrigerant enthalpy	kJ/kg
L	Distributor length	mm
m	Refrigerant mass flow rate	g/s
P	Pressure	kPa
Q	Heating power	W
STD	Standard deviation	-
T	Temperature	°C
x	Refrigerant quality	-
ε	Average performance indices	-

Subscripts

eri,i	Evaporator inlet, circuit i
ero,i	Evaporator outlet, circuit i
dri	Distributor inlet
i	Circuit i
l	Saturated liquid or liquid phase
m	Mass flow rate
v	Saturated vapor
xri	Expansion valve inlet
xro	Expansion valve outlet

Superscripts

*	Non-dimension value
---	---------------------

CHAPTER 1 INTRODUCTION

1.1 Refrigerant distributor in air conditioning system

Refrigerant distributor is not a necessary component for all air conditioning systems. It is usually used when evaporator size is large, but the tube diameter is small, in order to keep good heat transfer coefficient. In this case, distributor is used to increase the number of circuits so that the refrigerant pressure drop through evaporator is acceptable. A good distributor is supposed to separate two-phase refrigerant evenly into each circuit.

To achieve this purpose, several different designs have been put forward. The first type is the nozzle distributor which uses a sharp-edged orifice to increase the velocity of two-phase fluid and creates homogeneous flow before the fluids enter different circuits. Figure 1 shows the inner structure of a nozzle type distributor with an orifice which can be permanent or replaceable. The replaceable orifice is convenient if the system needs to be operated with different refrigerants, load, and different circuit numbers. The second type is Venturi distributor as shown in Figure 2. It utilizes a contoured throat to replace the orifice in nozzle type distributor. When two-phase fluid passes through the throat, its pressure decreases while velocity increases, which will make the liquid and vapor mix completely. Compared to the nozzle type distributor, the Venturi distributor causes a lower pressure drop and can work in a wider range of capacity [1]. These two types are similar in principle because both mix two-phase flow by increasing the flow velocity and then distribute. There is another type of distributor which is operated under a different mechanism, as shown in Figure 3. When two-phase flow enters this distributor, liquid phase stays at bottom while vapor phase at the top. Then, both liquid and vapor will be pushed down evenly into each circuit through the slots.

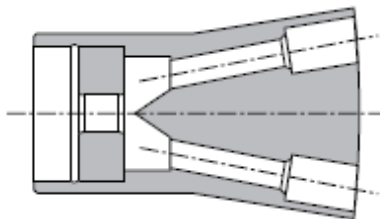


Figure 1 Structure of the nozzle type distributor [2]

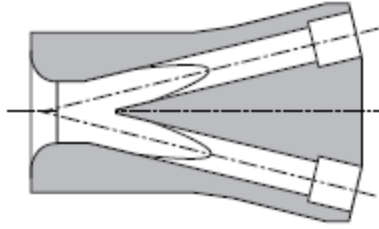


Figure 2 Structure of Venturi distributor [2]

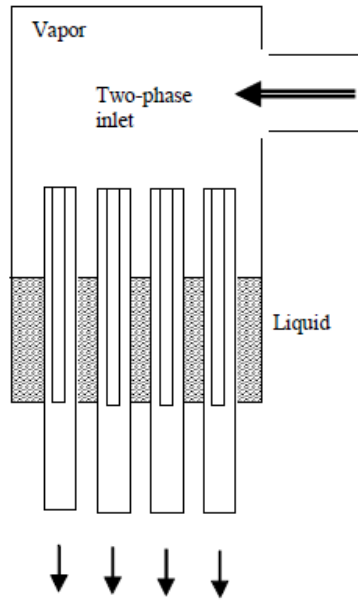


Figure 3 Structure of distributor with the mechanism of separating and then distributing [3]

Although various types of distributors have been designed with the purpose of dividing two-phase flow uniformly into each circuit, it is nearly impossible to achieve perfect distribution in practice. Maldistribution always happens to different degrees with some circuits being flooded while others being dried out. This scenario reduces the overall heat transfer coefficient of the heat exchanger and influences the system performance.

1.2 Literature review

To get a better understanding about two-phase flow behavior in distributors and therefore improve its performance, many researches have been done for different types of distributors by experiments as well as simulations.

1.2.1 Experiment investigation

Chen [4] explored the effects of installation angle, load conditions, and feeder tube lengths on the performance of a distributor with throttle. Based on his results, the mounting orientation and loading conditions are not the main reasons for the maldistribution, while the difference in feeder tube length plays an important role in flow uniformity. Nakayama et al. [5] studied the influence of mass flow rate, distributor inlet quality, inclination angles and geometry on distribution for distributor with orifice. Electrical heaters were used to evaporate two-phase refrigerant to superheated state with a constant superheat of 10 K at the outlets. The maximum cooling capacity difference was used as the criterion to evaluate the uniformity of distribution. It was found that larger L/D and higher quality can result in better distribution while mass flow rate almost has no effect. It also indicated that for distributor with larger L/D, distribution is less sensitive to inclination angle. Liang et al. [6] investigated a pressure drop type distributor with R22 as working fluid. They focused on the influence of inclination angle and liquid phase superficial velocity. It was concluded that vertical installation can guarantee better distribution and dispersed flow (liquid phase superficial velocity larger than 10^7 kg/m²h) at the inlet of distributor is preferred than annular flow. Mao et al. [7] compared three different distributor configurations (Venturi distributor connected with smooth tube, Venturi distributor connected with internally spirally micro-finned tube and distributor within a roller) and evaluated their performance by the distribution of temperature and pressure at the exit of each branch. It was found that Venturi distributor connected with internally spirally micro-finned tube can achieve the most uniform distribution and has larger COP compared with the other two types, which suggested that the flow regime at the inlet of distributor is significant to the distribution. It was also noticed that larger mass flux will produce bad distribution. Fay [3] studied the effect of refrigerant maldistribution and airside maldistribution on the evaporator and system performance for a conical distributor. The change in superheat pattern was not obvious with various mass fluxes, distributor inlet qualities and inclination angles, which indicated that the refrigerant maldistribution happened not because of the phase separation but some other reasons. It was found that maldistribution of refrigerant can cause a decrease of 4% in COP and 5% in capacity and the airside maldistribution has a bigger impact on system COP than capacity. Bowers et al. [8] achieved an improvement in refrigerant distribution by using an distributor integrated with expansion device which can limit the phase-separation to some degree.

Compared with the traditional distributors, the new integrated distributor has a more uniform mass flow rate and superheat under several different working conditions.

Yoshioka et al. [9] evaluated the performance of a cylinder-type distributor by analyzing the distribution of inlet quality and flow rate at each branch. By optimizing the distributor geometries, the uniformity of refrigerant quality and mass flow rate were greatly improved. Zhang et al. [10] studied the influence of several nonstructural factors on a reservoir type distributor. For this type of distributor, the structure of inlet tube has negligible effect on distribution, while the orientation is of great importance. And, the distribution is more sensitive to refrigerant mass flow rate than quality. Han et al. [11] compared the performance of reservoir type distributor with cyclone type and jet type distributor in a R410A system. It was proved that the reservoir and jet type distributor perform better than the cyclone distributor. For all the three types, distribution under larger mass flow rates is more uniform. Zhang et al. [12] investigated the performance of a double-barrel distributor which is similar but has a better performance than the reservoir type distributor. The double barrel design can alleviate maldistribution due to low velocity suffered by reservoir type distributor. With the increase of mass flow rate, distribution performance was improved because of the higher refrigerant speed. Wang et al. [13] studied several influential factors on flow distribution in a reservoir-type distributor. It was found that a longer inlet tube was better because it reduced the phase separation after an elbow in the inlet tube. Similar with other researches, it also suggested that vertical installation was preferable to avoid the effect of gravity. A compensation method was put forward to achieve better distribution by matching feeder tube length according to non-uniform air flow condition.

Choi et al. [14] studied the effect of refrigerant maldistribution on finned-tube evaporator. It was indicated that part of the reduction in capacity is a result of internal heat transfer among different circuits. Liang et al. [15] conducted experiments with a wheel distributor and found that distribution is only related to the ratio of the length of branch channel to the distributor circumference, and not influenced by fluid velocity, flow pattern or rotation speed of the wheel distributor. Li et al. [16, 17] experimentally evaluated the performance of distributors with three different bases: sharp-end base, cone-shaped base, and spherical base. It was found that the spherical base distributor has the best performance, followed by cone base distributor, while the sharp-end base distributor is the worst. Ishii and Kazuki [18] as well as Ishikawa and Ishii [19] examined the performance of a distributor with a bend pipe at the inlet. It showed that the air-water

flow formed an annular pattern at the inlet pipe and the water film is thicker at the outer circumference of the bend pipe due to the centrifugal force, which is the main reason for maldistribution.

1.2.2 Numerical simulation

In addition to experiment, modeling is another useful tool to learn the behavior of refrigerant two-phase flow in distributor. Chen [4] developed a model to predict refrigeration distribution based on Baroczy pressure drop model and Henry-Fauske critical flow model. It was proved to be good at not very high flow rate. Li et al. [20] built two models for two-phase flow in refrigerant distributor with FLUENT and PHOENICS codes and compared the results with experiment data in literature. Both models can work well for a typical distributor geometry. Li et al. [16, 17] applied the validated FLUENT model developed by Li et al. [20] to evaluate the performance of five types of distributors with different bases. For most of the cases, spherical base distributor is better than other types and it is recommended to make the orifice close to distributor base. Ishii and Kazuki [18] and Ishikawa and Ishii [19] developed a particle/grid hybrid model to simulate gas-liquid flows in distributor with bend pipes at the inlet. The simulation results indicated that liquid film at the outer circumference was thicker because of the centrifugal force, which agreed well with the experiment results. Based on the model developed previously [18], Ishii et al. [21] further studied the effects of the gravity and connecting angle of the bend pipe before distributor on distribution. It showed that gravity plays an important role in liquid distribution and smaller connecting angle tends to cause bad distribution. Han et al. [11, 22] applied k-epsilon and Eulerian multiphase model to simulate refrigerant two-phase flow in three types of distributor. The flow field inside distributor was obtained, which can reveal flow pattern and quality distribution. Zhang et al. [12] analyzed the influence of geometry on double-barrel type distributor by FLUENT model. It indicated that the distributor height has a larger influence on distribution than diameter, by which the optimized distributor can be designed. Kaern et al. [23-25] numerically investigated the effect of air and refrigerant maldistribution on capacity, and then analyzed several possible sources for maldistribution. It was concluded that by controlling the same superheat for each circuit, the capacity degradation due to maldistribution was compensated. Kim et al. [26, 27] evaluated a hybrid method to balance refrigerant flow in multi-circuit evaporator by modeling. The effect of void fraction, feeder tube geometry, and upstream vs. downstream control was investigated. Heikal

[28] studied two-phase flow distribution using FLUENT and found that orifice is not always good for distribution.

CHAPTER 2 EXPERIMENT SETUP

2.1 Facility

The experiment facility built for this study is shown in Figure 4 and Figure 5. It consists of two parts: condensing unit and test section. Condensing unit includes condenser, compressor, sub-cooler, accumulator and receiver, and the test section is composed of thermal expansion valve, distributor and evaporator. R134a was used as working fluid.

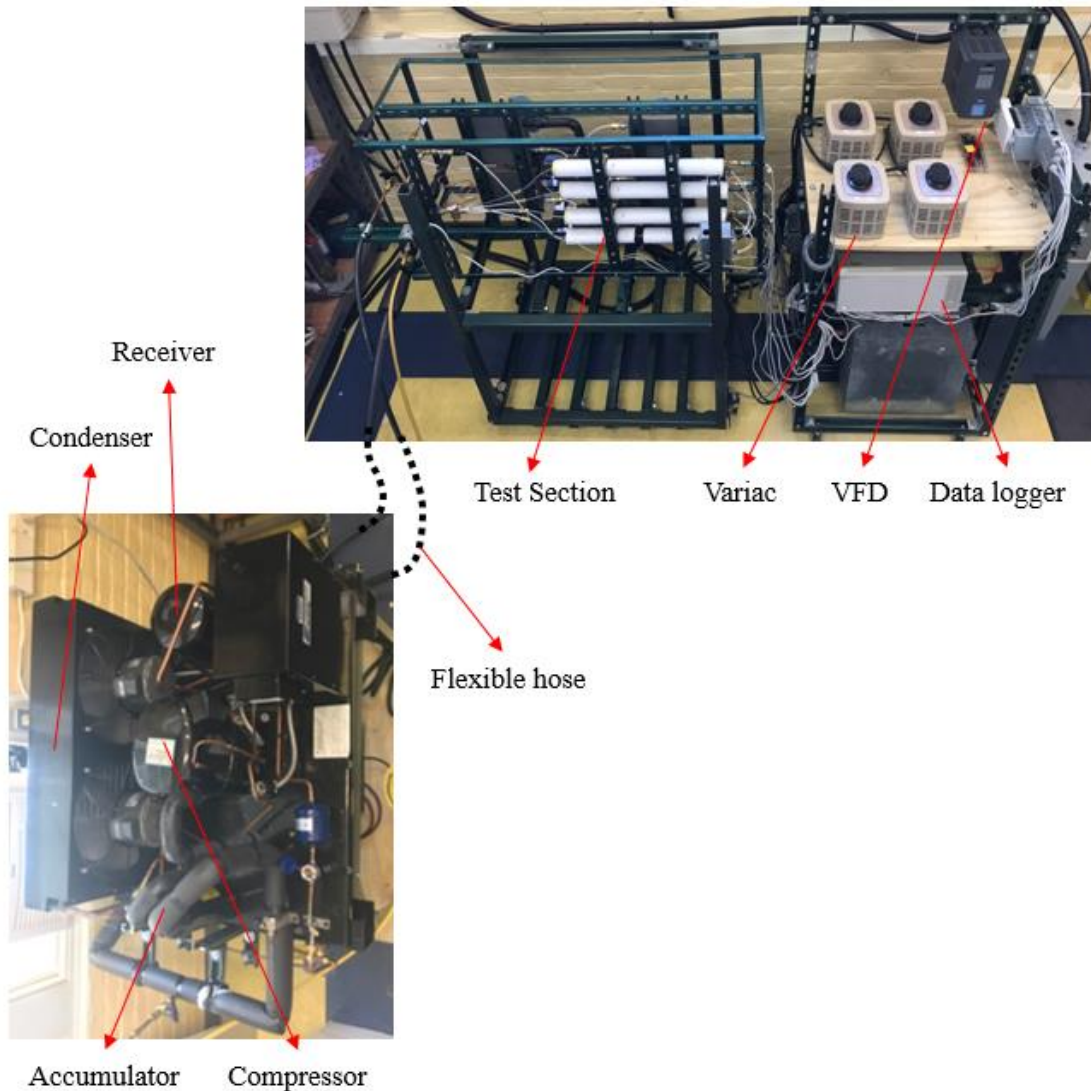


Figure 4 Experimental facility

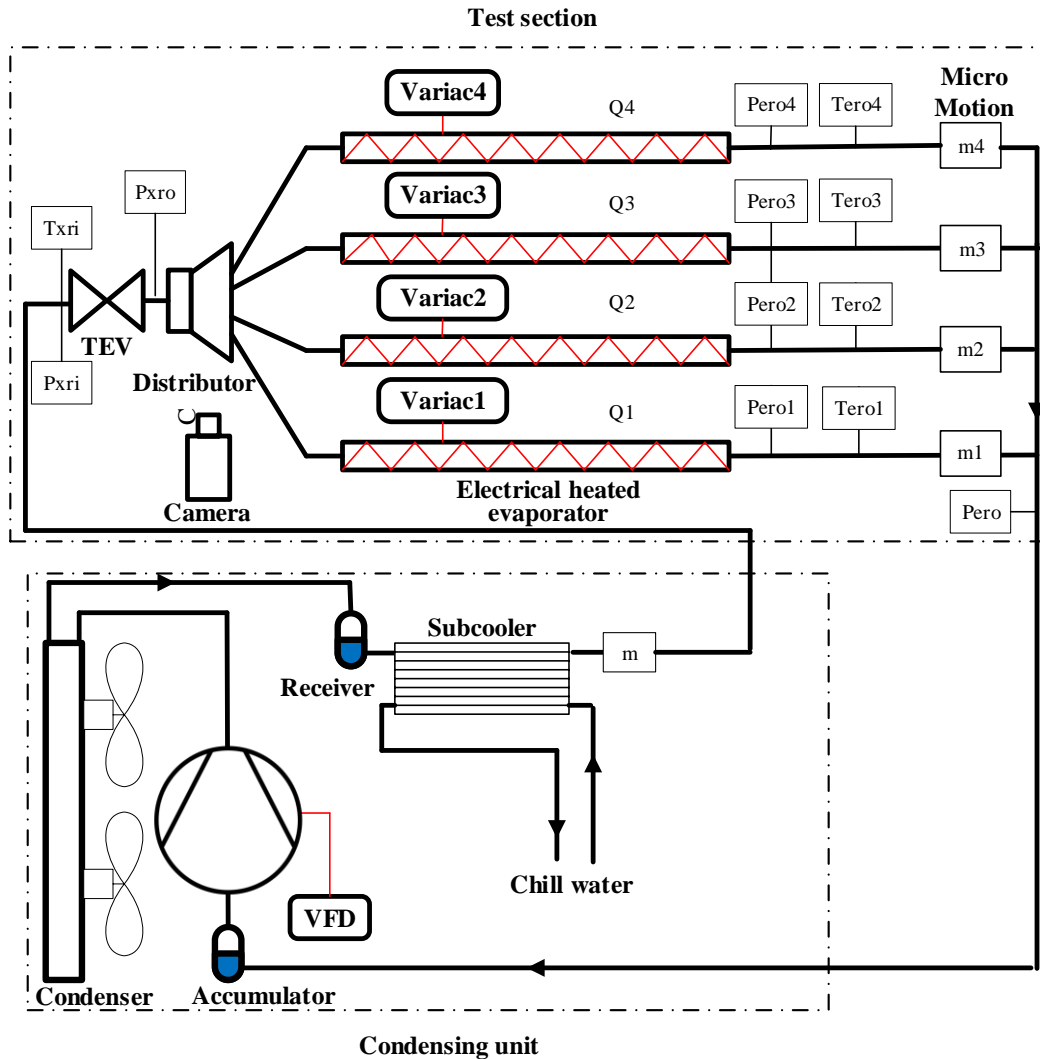


Figure 5 Schematic drawing of experimental facility

The compressor is controlled by a VFD to change the operating frequency, so that the refrigerant mass flow rate can be adjusted. POE 32 oil is used in the compressor which is compatible with R134a. The condenser is cooled by air flow which is provided by two paralleled fans. To change the refrigerant quality at the inlet of distributor, a sub-cooler was installed after the condenser. By changing the mass flow rate of chilled water in sub-cooler, refrigerant quality can be adjusted. At the downstream of the sub-cooler, a Micro Motion was installed to measure the total mass flow rate of refrigerant. The thermal expansion valve and distributor used in this study were provided by Parker Hannifin, designed with a nominal capacity of 1.5 tons as shown in Figure 6. Instead of using a real evaporator, an electrical heated evaporator was designed for this system so that the capacity of each circuit can be controlled and measured separately. A schematic drawing of the

evaporator is shown in Figure 7. The electrical heater was inserted into a copper tube concentrically, with a spiral-structured wire surrounded at the outside surface of the heater to distribute two-phase refrigerant evenly between the heater and copper tube and avoid local dry out. High-temperature fiberglass insulation was wrapped at the outside of evaporator to eliminate heat leaks. Four Micro Motions were installed at each circuit downstream of the evaporator to measure the mass flow rates separately. The test section was built in such a way that the whole structure can be placed in any orientations while the connection between expansion device, distributor and evaporator keep the same. This guaranteed that the influence of orientation can be investigated excluding the disturbance due to change in tube connections.



Figure 6 thermal expansion valve and distributor assembly

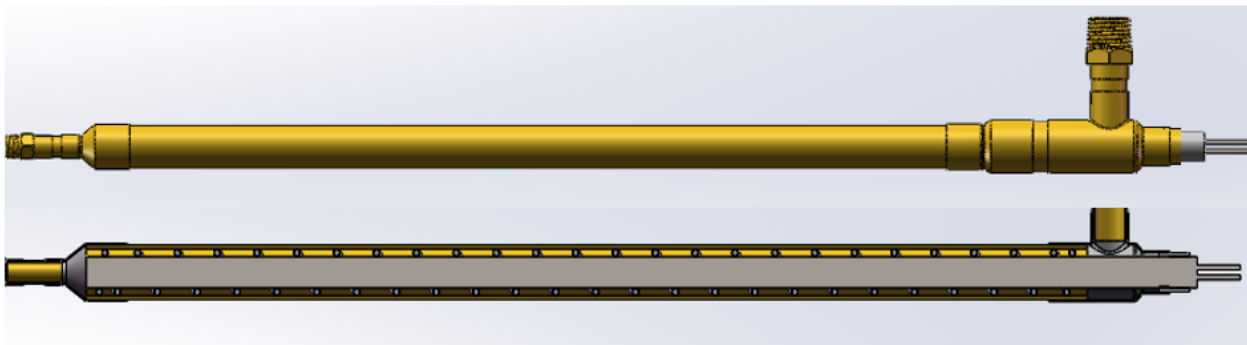


Figure 7 Schematic drawing of the evaporator

To get a better understanding about the behavior of refrigerant two-phase flow in distributor, a transparent version was built by 3D-printing based on the dimension of the original distributor from Parker Hannifin. As shown in Figure 8, the transparent distributor is directly connected to the body of expansion valve by bolts and sealed with O-Ring. Clear and flexible PFA tubes were glued to distributor outlets and connected to evaporator inlets on the other ends.

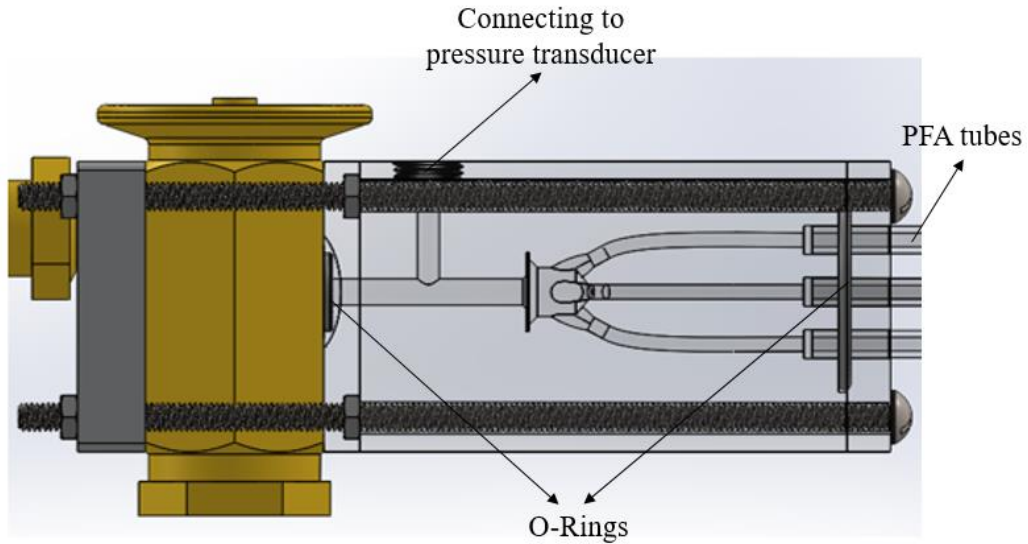


Figure 8 Transparent distributor and TEV assembly

2.2 Experiment procedures and conditions

- Set up system total mass flow rate by controlling the compressor frequency with VFD.
- Adjust distributor inlet quality by controlling the flow rate of chilled water in sub-cooler.
- The evaporation pressure (P_{ev} in Figure 5) is set to be a constant for all working conditions by controlling compressor frequency and the opening of expansion valve.
- Adjust each variac individually to change the heat input of each electrical heater, so that the same superheat is achieved at the exits for all circuits.
- When system became stable, write data in LabView, at the same time, take video from high-speed camera.

Experiment conditions are listed in Table 1.

Table 1 Experiment conditions

Working fluid	R134a
Mass flow rate	15, 20, 25 g/s
Distributor inlet quality	0.08, 0.15, 0.23
Orientations	Horizontal, vertical upwards, vertical downwards

Table 1 Experiment conditions (cont.)

Pero	380 kPa
Superheat at evaporator exit	About 10 °C

2.3 Data reduction and uncertainty

As shown in Figure 5, temperature and pressure at the exit of each circuit are measured by thermocouples and pressure transducers. Based on these parameters, refrigerant enthalpy can be calculated by REFPROP:

$$h_{ero,i} = f(P_{ero,i}, T_{ero,i}) \quad (1)$$

where i represents one of the circuits ($i = 1$ to 4).

To get the heat load of each electrical heater, four watt-transducers were used. The mass flow rate of each circuit is also available through Micro Motion. So, the refrigerant enthalpy at evaporator inlet can be calculated from the following equation:

$$h_{eri,i} = h_{ero,i} - \frac{Q_i}{m_i} \quad (2)$$

where $h_{eri,i}$ and $h_{ero,i}$ are refrigerant enthalpy at evaporator inlet and outlet of circuit i , Q_i is heat load of circuit i , m_i is mass flow rate of circuit i .

Refrigerant quality at evaporator inlet is obtained by equation (3):

$$x_{eri,i} = \frac{h_{eri,i} - h_l}{h_v - h_l} \quad (3)$$

where h_l and h_v are enthalpy of saturated liquid and vapor refrigerant at evaporation pressure.

On the other hand, temperature and pressure before expansion valve and the pressure after expansion valve are measured. So, the refrigerant quality at distributor inlet also can be obtained by REFPROP:

$$x_{dri} = f(T_{xri}, P_{xri}, P_{xro}) \quad (4)$$

To check the reliability of measurement, we can calculate the mass flow rate of liquid phase refrigerant after expansion valve by two different methods, and then compare the difference between these two results. The reason to compare this parameter is because all the directly measured parameters are involved to calculate the quality at the inlet and outlet of distributor as shown in equation (3) and (4). It is unreasonable to directly compare the quality, instead we compare the mass flow rate of liquid phase refrigerant at inlet and outlet of distributor.

$$m_l = m(1 - x) \quad (5)$$

One set of data from experiment is taken as an example to show the details. Table 2 shows the calculation based on method 1 with measured parameters shown in the blue frame in Figure 9, and Table 3 shows the calculation based on method 2 with measured parameters shown in the red frame in Figure 9. All the calculated parameters are obtained from equations (1) to (5). When all $m_{l,i}$ (circuits 1 to 4) from Table 3 are added together and compared with m_l from Table 2, the difference is only $\pm 0.96\%$, which indicates a good accuracy of measurement. The uncertainty for measured parameters is presented in Table 4.

Table 2 Parameters for method 1 to calculate mass flow rate of liquid phase refrigerant before distributor

Measured Parameters				Calculated Parameters	
T_{xri} (°C)	P_{xri} (kPa)	P_{xro} (kPa)	m (g/s)	x_{dri} (-)	m_l (g/s)
46.77	1460.96	650.85	19.9660	0.1853	16.2666

Table 3 Parameters for method 2 to calculate mass flow rate of liquid phase refrigerant after distributor

Circuits	Measured Parameters				Calculated Parameters			
	$P_{ero,i}$ (kPa)	$T_{ero,i}$ (°C)	Q_i (W)	m_i (g/s)	$h_{ero,i}$ (kJ/kg)	$h_{eri,i}$ (kJ/kg)	$X_{eri,i}$ (-)	$m_{l,i}$ (g/s)
1	593.44	27.22	771.85	4.9108	416.37	259.19	0.1634	4.1082
2	541.61	27.29	777.11	5.2944	417.64	270.86	0.2296	4.0787
3	594.44	24.92	777.87	4.8084	414.06	252.29	0.1267	4.1991
4	587.97	24.78	774.91	4.9912	414.09	258.84	0.1593	4.1960

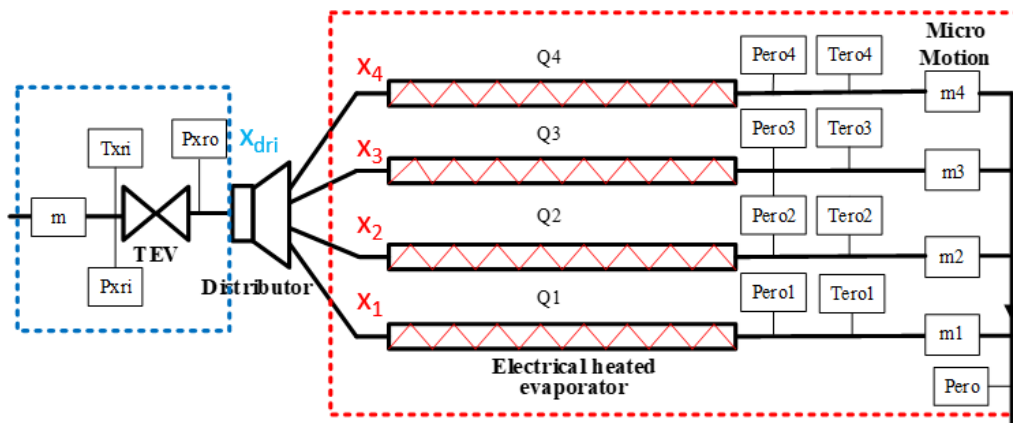


Figure 9 Parameters measured in this study

Table 4 Uncertainties of measurement

Measurement	Sensors	Unit	Uncertainty
Temperature	Sheathed T-type thermocouple	°C	±0.34
Pressure	Pressure transducer PSPT0150SVSP-S and PSPT0500SVSP-S	kPa	±3.56

Table 4 Uncertainties of measurement (cont.)

Mass flow rate	Coriolis mass flow meter	g/s	$\pm 0.5\%$
Heating power	Watt transducer PC5-002E and H2BT/100K	W	± 5

CHAPTER 3 EXPERIMENT RESULTS UNDER DIFFERENT WORKING CONDITIONS

Although each distributor is designed for a corresponding working condition, refrigeration systems often need to operate over wide ranges of temperature and satisfy various load requirements. In some cases, due to space limitation, distributors have to be installed in a certain orientation. To understand how the variation in working conditions influences the performance of refrigerant distributor, a series of experiments were conducted with the facility described in chapter 2. The effect of refrigerant mass flow rate, distributor inlet quality and orientation were investigated in this study.

3.1 Effect of refrigerant mass flow rate

Figure 10 shows the distribution of mass flow rate and quality at three different mass flow rates (15, 20 and 25 g/s) while distributor inlet quality and orientation keep the same ($x=0.22$, horizontal orientation). The red line and blue line indicate the average mass flow rate and average quality, respectively. Figure 11 shows the front and side views of distributor and the configuration of circuits 1 to 4 corresponding to the numbers shown in Figure 10. For all the conditions, circuits 1 and 4 always have higher mass flow rate than average while quality is lower than average.

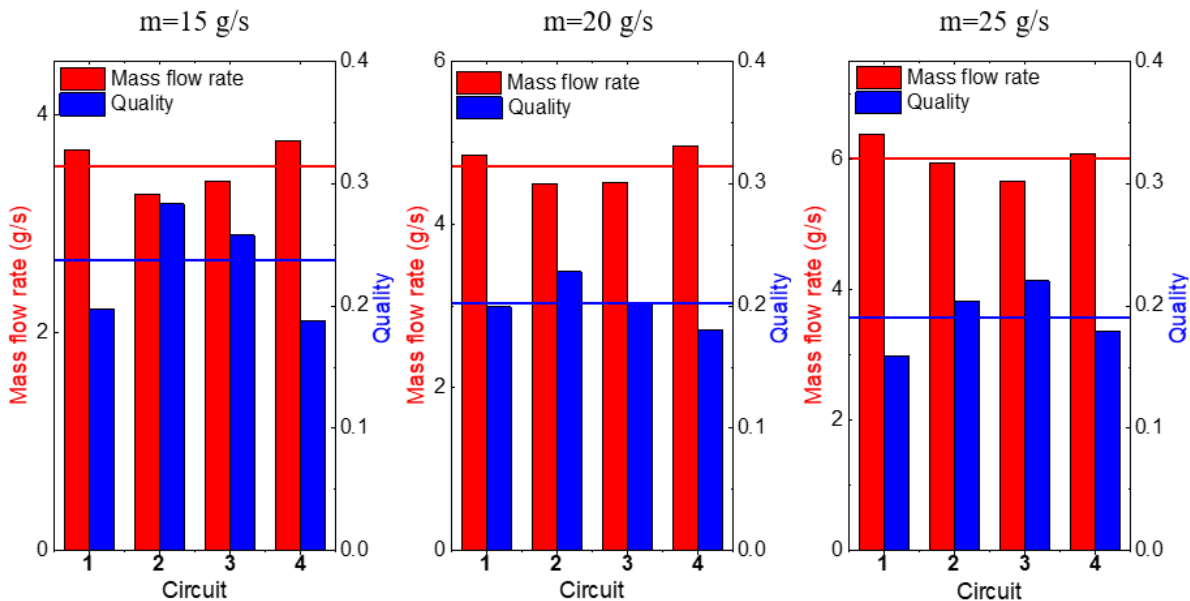


Figure 10 Distribution of mass flow rate and quality ($m=15$ g/s, $x=0.22$, horizontal)

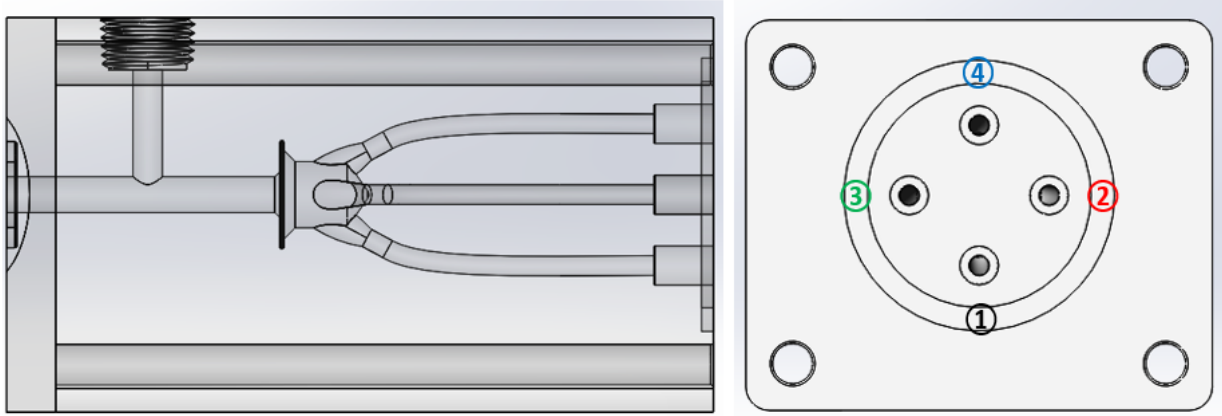


Figure 11 Front view and side view of the distributor

To compare results from different working conditions in one figure, non-dimensional mass flow rate (m_i^*), quality (x_i^*) and heat load (Q_i^*) are defined by the following equations:

$$m_i^* = \frac{m_i}{(\sum_{i=1}^4 m_i)/4} \quad (6)$$

$$x_i^* = \frac{x_i}{(\sum_{i=1}^4 x_i)/4} \quad (7)$$

$$Q_i^* = \frac{Q_i}{(\sum_{i=1}^4 Q_i)/4} \quad (8)$$

All the three parameters were used to indicate the performance of distributor. Distribution of mass flow rate shows how much refrigerant is divided into each circuit including both vapor and liquid phase, and distribution of vapor phase refrigerant is shown by non-dimensional quality. Since superheat at exits of evaporator for all circuits were controlled to be the same, circuit that gets more liquid will need more heat load. In other words, distribution of heat load reflects the distribution of liquid phase refrigerant, which is used to produce cooling capacity.

Figure 12 shows the distribution of non-dimensional mass flow rate, quality and heat load as a function of total mass flow rate at horizontal orientation with distributor inlet quality of 0.22. As the total mass flow rate increases, distribution of mass flow, quality and heat load are improved, which means better distribution can be obtained at higher mass flow rate. In horizontal orientation, circuits 1 and 4 are at bottom and top position respectively, and circuits 2 and 3 are at the middle.

It is noticed that circuit 1 and circuit 4 have higher mass flow rate and lower quality than circuit 2 and 3. So the performance of this distributor is not affected by gravity.

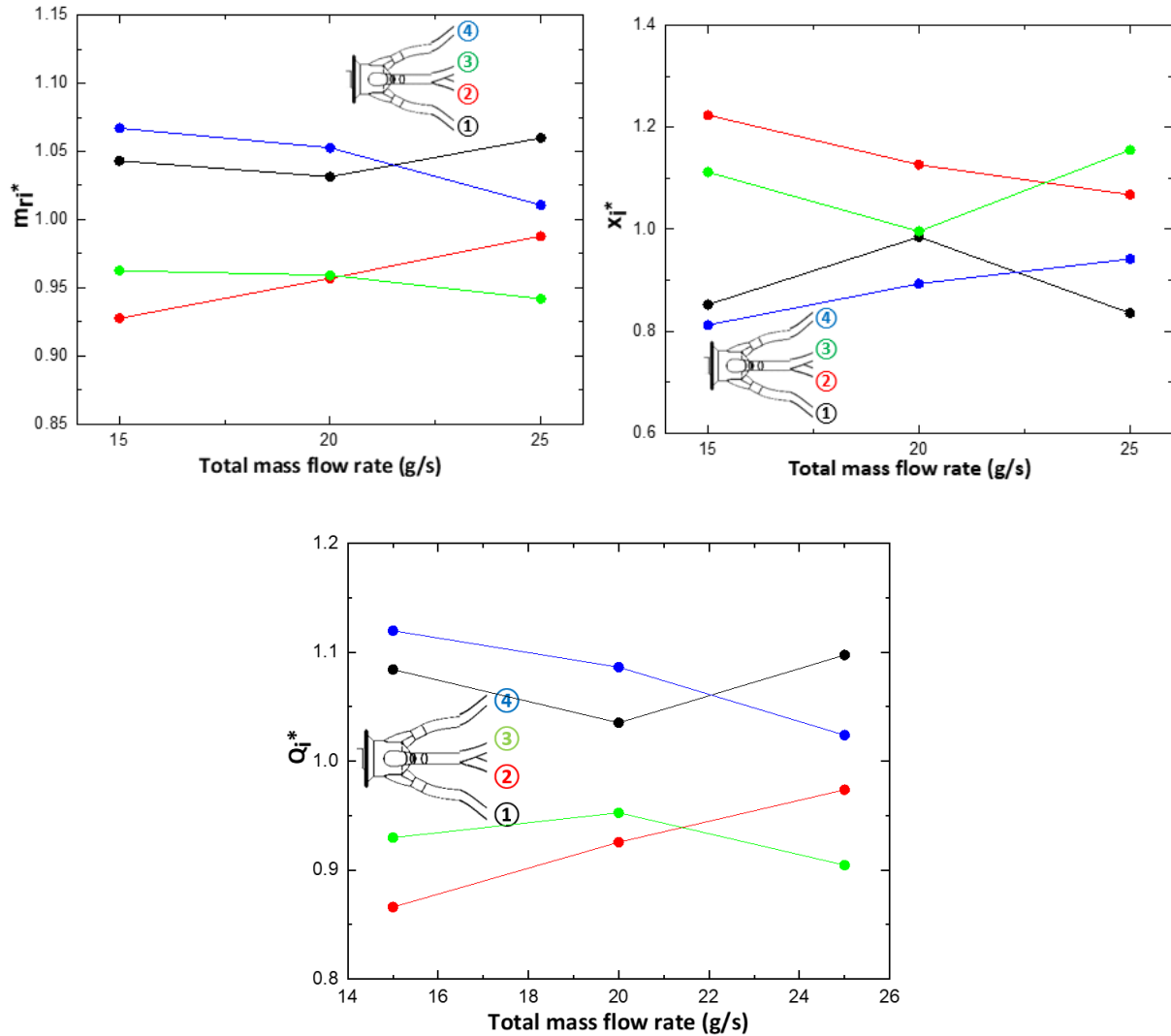


Figure 12 Distribution of non-dimensional mass flow rate, quality and heat load ($x=0.22$, horizontal)

Figure 13 and Figure 14 show the distribution of non-dimensional mass flow rate, quality and heat load as a function of total mass flow rate at vertical downward and upward orientation with distributor inlet quality of 0.22. In general, the distribution under different orientations has a similar pattern: circuits 1 and 4 always get more refrigerant than the other circuits. With the

increase of total mass flow rate, refrigerant distribution improved for all the conditions. This is because higher mass flow rate can increase the flow velocity. In consequence, liquid and vapor phase will mix thoroughly and distribute evenly into each circuit.

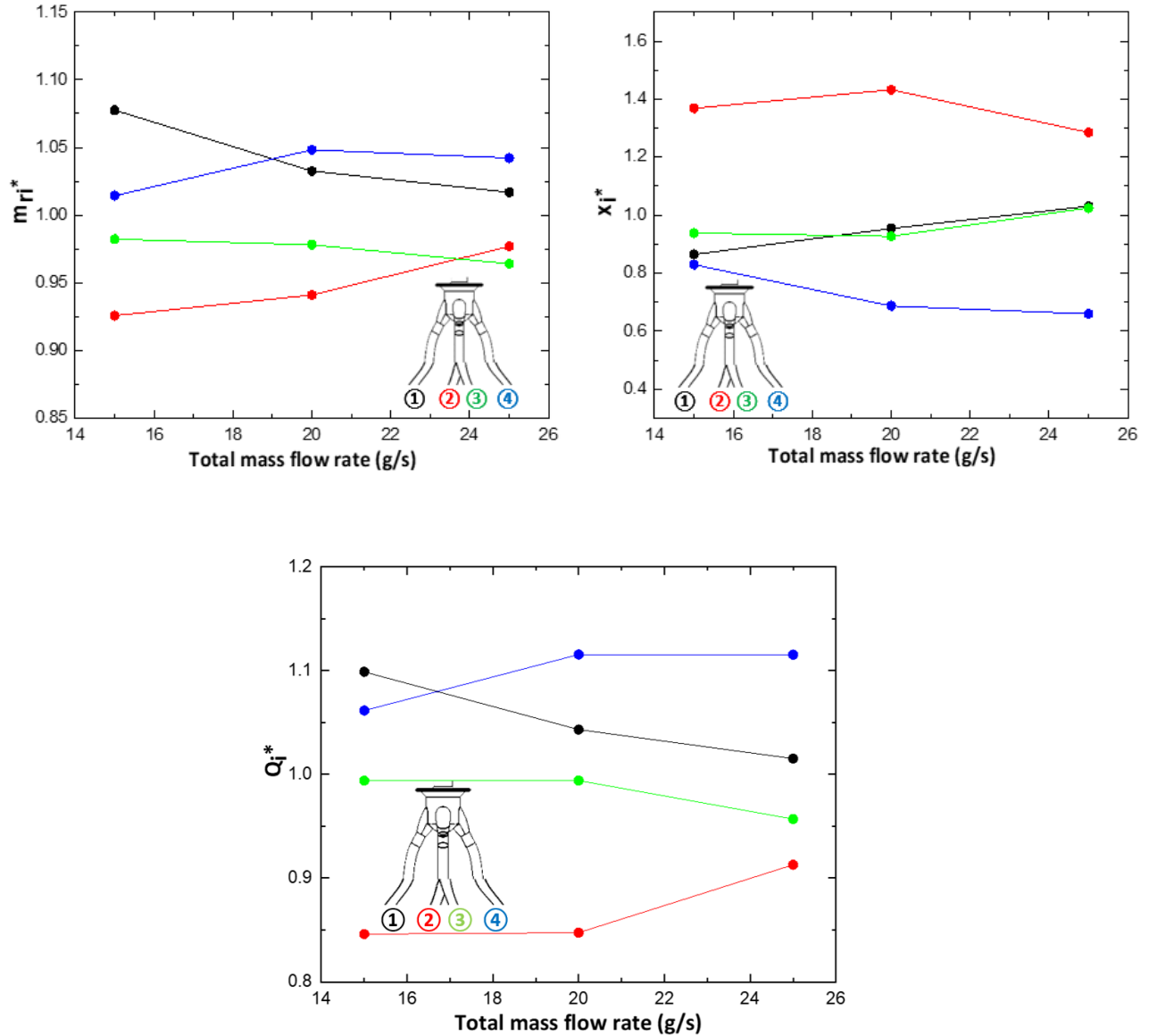


Figure 13 Distribution of non-dimensional mass flow rate, quality and heat load ($x=0.22$, vertical downward)

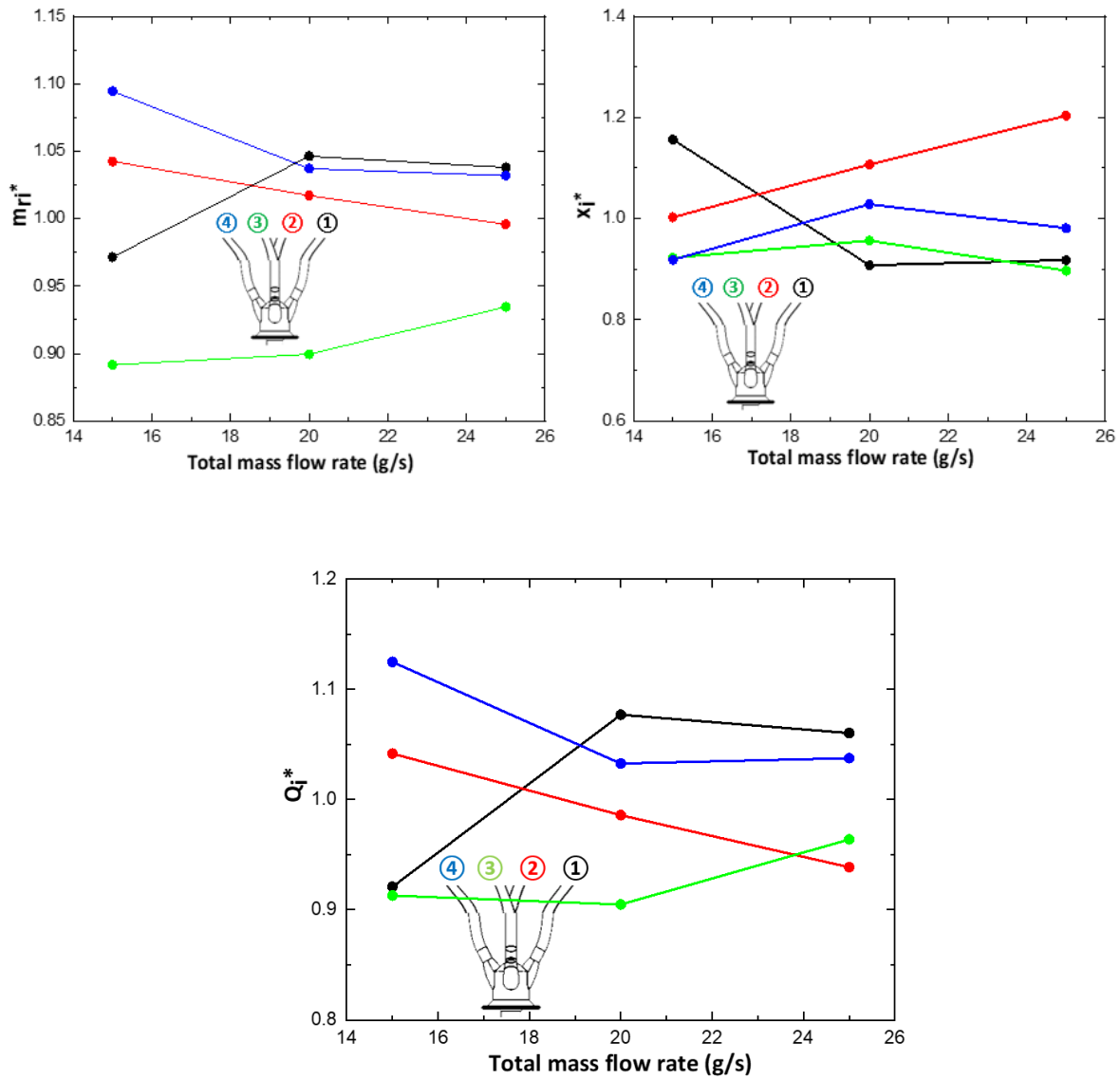


Figure 14 Distribution of non-dimensional mass flow rate, quality and heat load ($x=0.22$, vertical upward)

3.2 Effect of distributor inlet quality

Another factor influencing the performance of refrigerant distributor is quality. For a typical air conditioning and refrigeration system, refrigerant quality after expansion device is less than 0.3. In this study, the range of quality investigated is between 0.08 and 0.22. Figure 15 shows the

distribution of non-dimensional mass flow rate, quality and heat load as a function of distributor inlet quality at horizontal orientation. As the distributor inlet quality decreases, distribution of mass flow rate is improved, but distribution of quality shows an opposite trend. In this case, the distribution of heat load is regarded as the decisive criteria because it reflects the behavior of liquid phase refrigerant which is the useful part for cooling capacity. According to Figure 15, heat load is more uniform at lower inlet quality. But when the inlet quality is smaller than 0.15, the improvement due to decreasing in quality is not obvious any more.

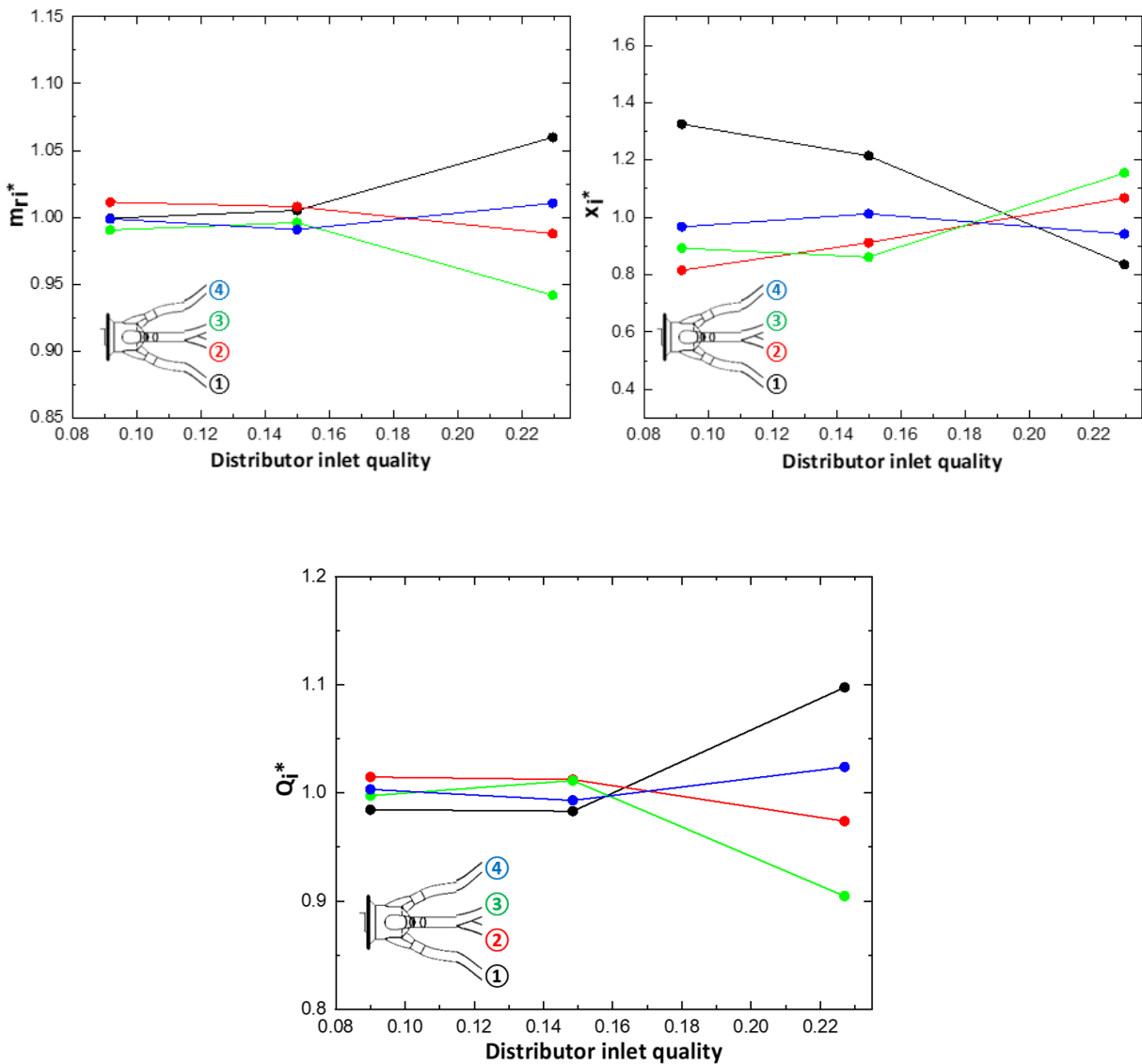


Figure 15 Distribution of non-dimensional mass flow rate, quality and heat load ($m=25$ g/s, horizontal)

Figure 16 and Figure 17 show the results for vertical downward and upward orientation. The conclusions are similar to what have been got for horizontal orientation, i.e., lower distributor inlet quality will result in better distribution. A possible reason is that at lower quality, the influence of vapor phase is small, and the fluid is more like single phase.

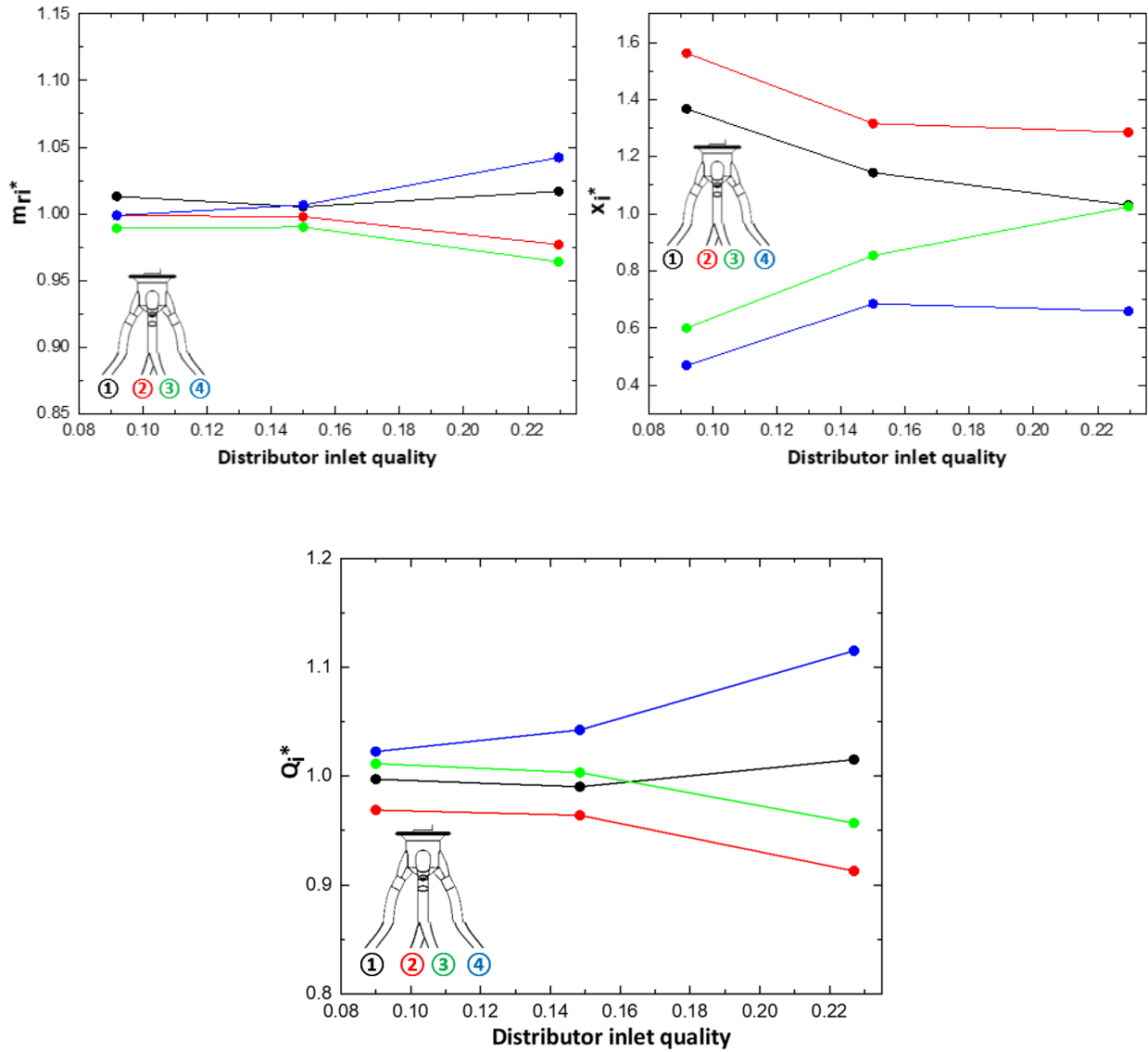


Figure 16 Distribution of non-dimensional mass flow rate, quality and heat load ($m=25$ g/s, vertical downward)

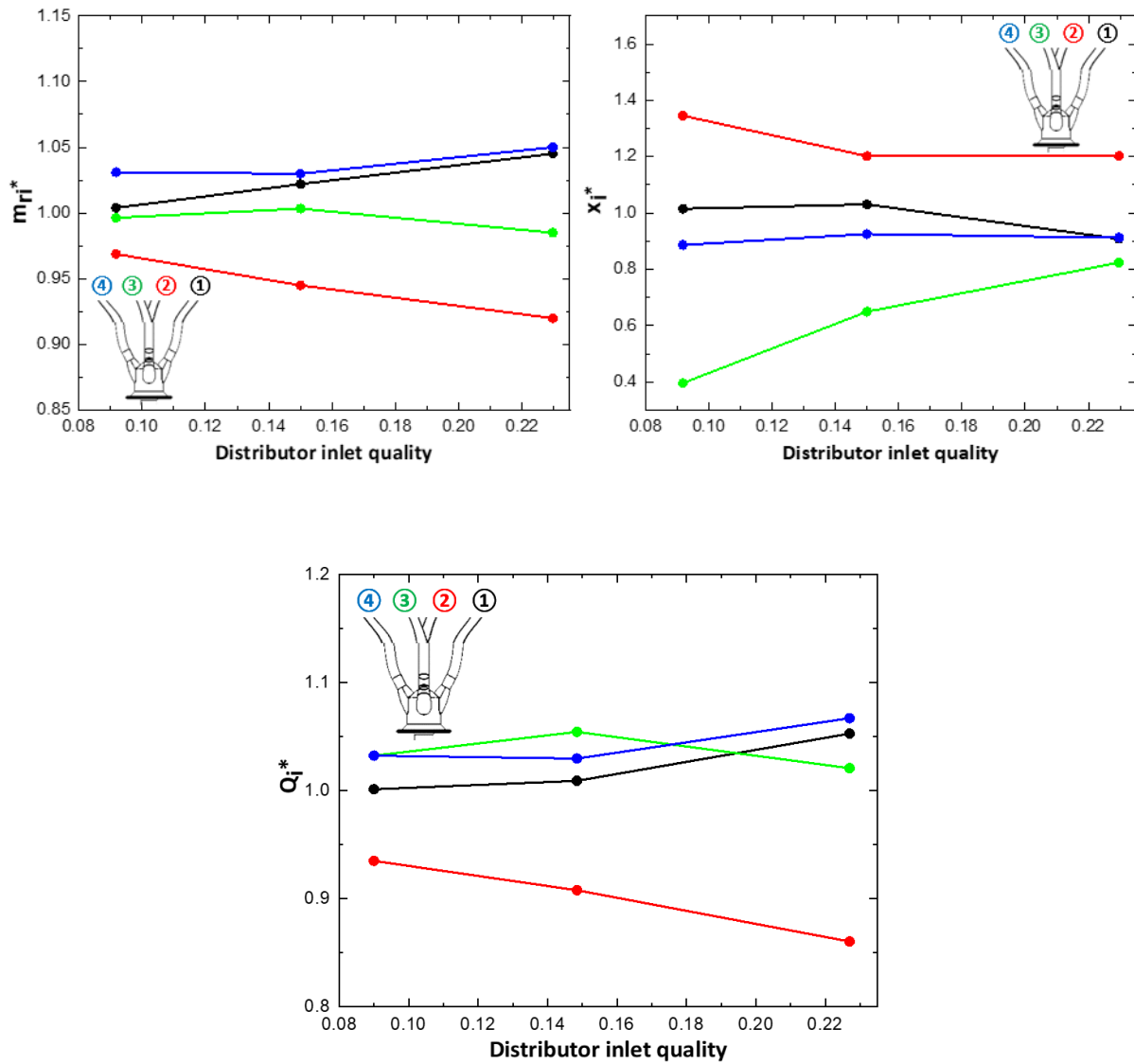


Figure 17 Distribution of non-dimensional mass flow rate, quality and heat load ($m=25$ g/s, vertical upward)

3.3 Effect of orientation

Due to space confinement, distributor needs to be installed in a certain orientation in some cases. For instance, distributors for air conditioning system used in vehicles are usually installed horizontally because of the limited space in vertical direction. On the other hand, distributors are

not always installed absolutely vertical or horizontal. What often happens is that there is a small inclination angle due to manual installation. In such cases, it is important to know if orientation will influence the performance of distributor.

In order to compare the distributor performance under different orientations in a single figure, a new parameter is defined by equation (9):

$$STD = \sqrt{\frac{\sum_{i=1}^4 (A_i^* - 1)^2}{4}} \quad (9)$$

where A_i^* represents the non-dimensional mass flow rate (m_i^*), quality (x_i^*), or heat load (Q_i^*) defined by equation (6) - (8). The standard deviation (STD) indicates dispersion of a set of data with respect to the average value. In other words, smaller standard deviation means more uniform distribution.

Figure 18 and Figure 19 show the standard deviation of mass flow rate (black lines), heat load (red lines) and quality (blue lines) under three orientations as a function of total mass flow rate (Figure 18) and distributor inlet quality (Figure 19). Although $STD(x)$ is not similar for different orientations, the results of $STD(m)$ and $STD(Q)$ are quite close to each other, which means orientation almost has no influence on distribution. It also verifies the conclusions from section 3.1 and 3.2 that larger mass flow rate and lower quality result in better distribution.

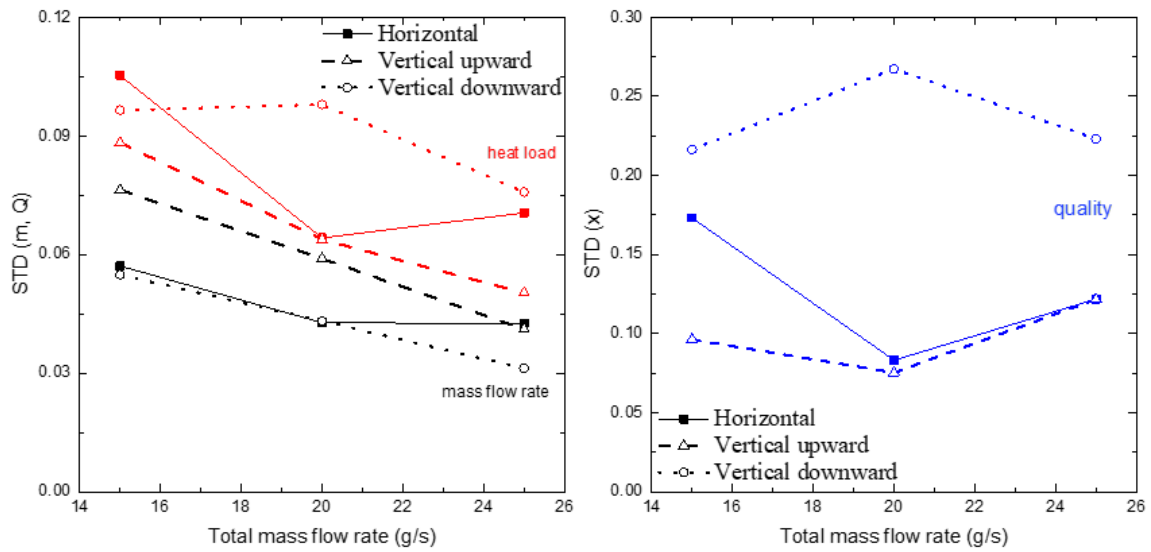


Figure 18 Standard deviation of mass flow rate, heat load and quality as a function of total mass flow rate

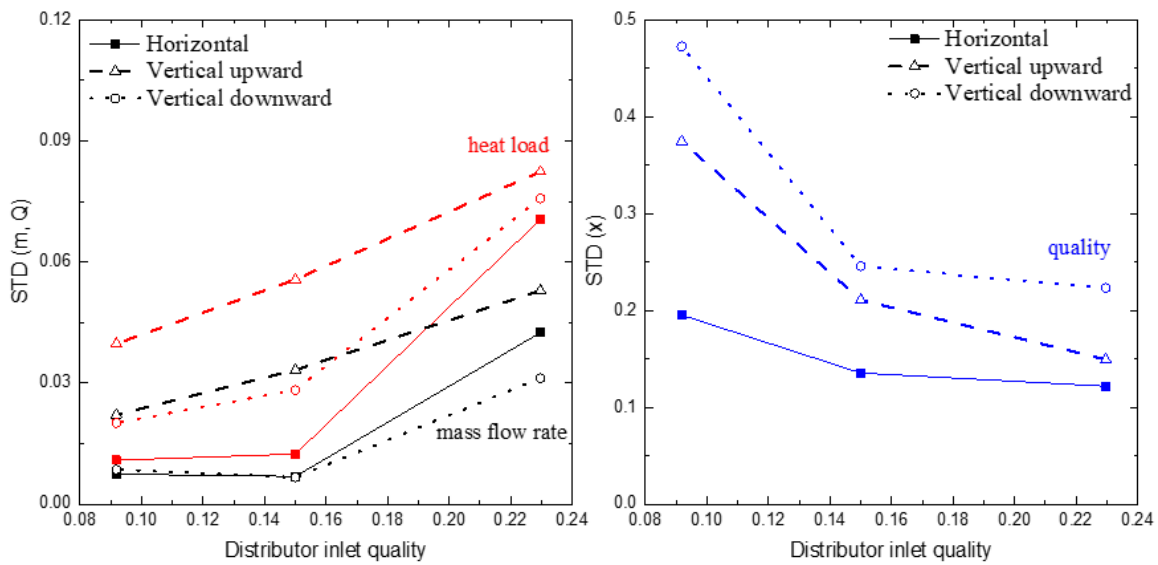


Figure 19 Standard deviation of mass flow rate, heat load and quality as a function of distributor inlet quality

CHAPTER 4 COMPARISON WITH REAL SYSTEM

The experiment facility used in this study includes all the components of a typical air conditioning system: compressor, condenser, expansion device and evaporator. However, it is different from real system in some respects so that more parameters can be measured, and the test section can be put in any orientations. The influence caused by these differences will be analyzed in this chapter.

4.1 Influence of pressure drop from Micro Motion on distribution

For a typical multi-circuit evaporator in air conditioning system, refrigerant from different circuits will enter a manifold right after the evaporator. However, for the evaporator in this study, as shown in Figure 20, refrigerant from each branch will pass through Micro Motions separately before converging in the manifold. An extra pressure drop is produced when superheated vapor-phase refrigerant flows through the Micro Motions. In order to investigate the extra pressure drop due to Micro Motion improves or deteriorates the refrigerant distribution, a set of experiments without Micro Motion were conducted.

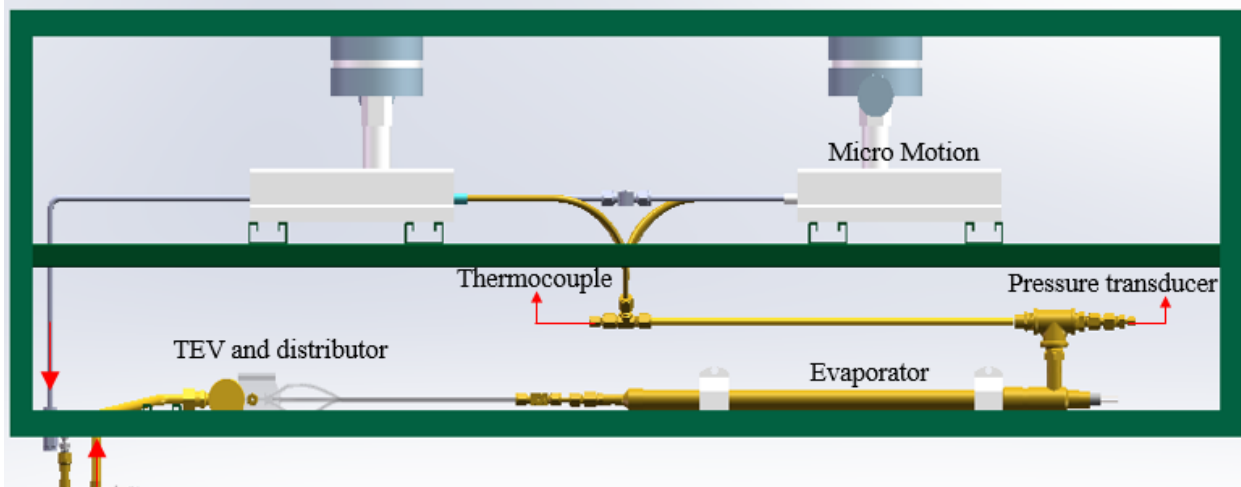


Figure 20 Top view of the test section in this study

Figure 21 shows the measured pressures at three different locations: before distributor (P1), exit of evaporator (P2), and after Micro Motions (P3). For all the experiments with Micro Motion, P3 was set to be a constant, but P1 will change with different mass flow rates. When Micro Motions

were bypassed, P1 was controlled to have the same value as the experiments with Micro Motion for each corresponding working condition. According to Figure 21, pressure drop between P1 and P2 is similar for experiments with and without Micro Motion, but in the situation without Micro Motion, pressure drop between P2 and P3 is greatly reduced.

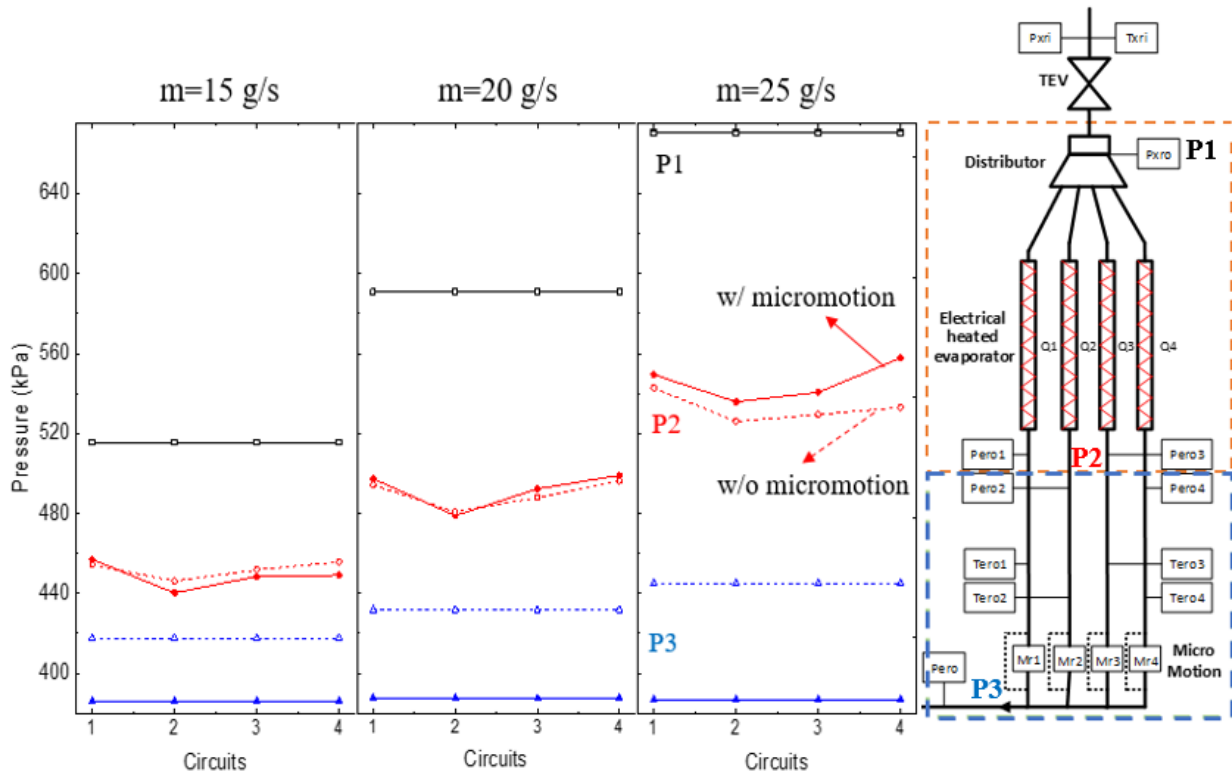


Figure 21 Measured pressure at three different locations

For experiments without Micro Motion, mass flow rate of each circuit is not available, therefore, refrigerant quality at evaporator inlet cannot be calculated neither. The distribution of heat load is used as the only parameter to indicate the performance of distributor. Figure 22 compares the distribution of non-dimensional heat load with and without Micro Motion. The dash lines relate to experiments without Micro Motion and solid lines represent results with Micro Motion. At lower mass flow rates (15 and 20 g/s), both the top line (blue) and bottom line (red) move far from the center, which means worse distribution when Micro Motions were bypassed. When mass flow rate increases to 25 g/s, the difference between two sets of experiments is negligible. Figure 23 compares the standard deviation of heat load without Micro Motion in vertical downward orientation with the results with Micro Motion under three orientations. It verifies the conclusion from Figure 22 that the existence of Micro Motions improves the refrigerant distribution.

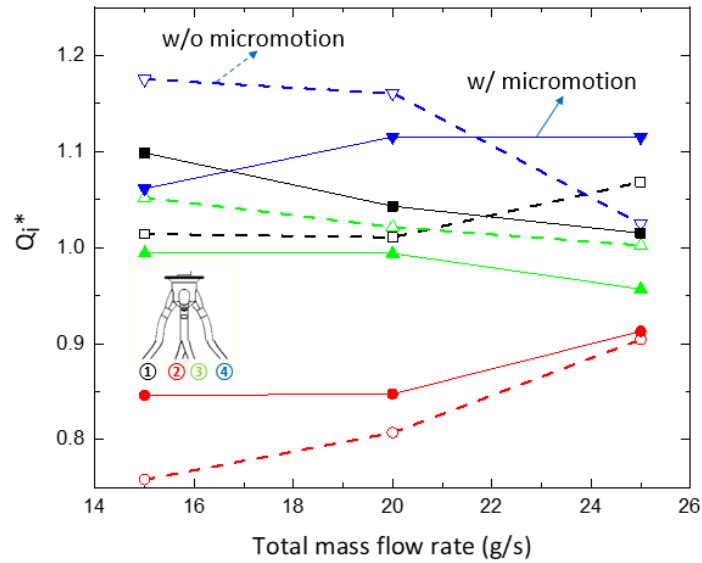


Figure 22 Distribution of non-dimensional heat load with and without Micro Motion ($x=0.22$, vertical downward orientation)

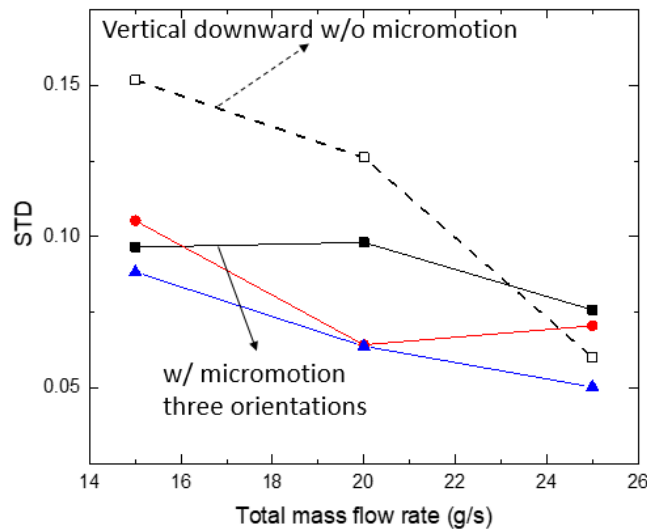


Figure 23 Standard deviation of heat load with and without Micro Motion

To explain the influence of Micro Motion on refrigerant distribution, pressure drop between distributor inlet and Micro Motion outlets is analyzed individually for each component. As shown in Figure 24, pressure drop in this range is divided into four parts: pressure drop in distributor ($\Delta P1$), pressure drop in feeder tubes ($\Delta P2$), pressure drop in evaporator ($\Delta P3$) and pressure drop in Micro Motions as well as the copper tubes ($\Delta P4$). From $\Delta P1$ to $\Delta P3$, it is two-phase pressure

drop, while ΔP_4 is only vapor phase pressure drop. The summation of ΔP_1 to ΔP_4 is the same for each circuit, but it may be different in one or more of the components.

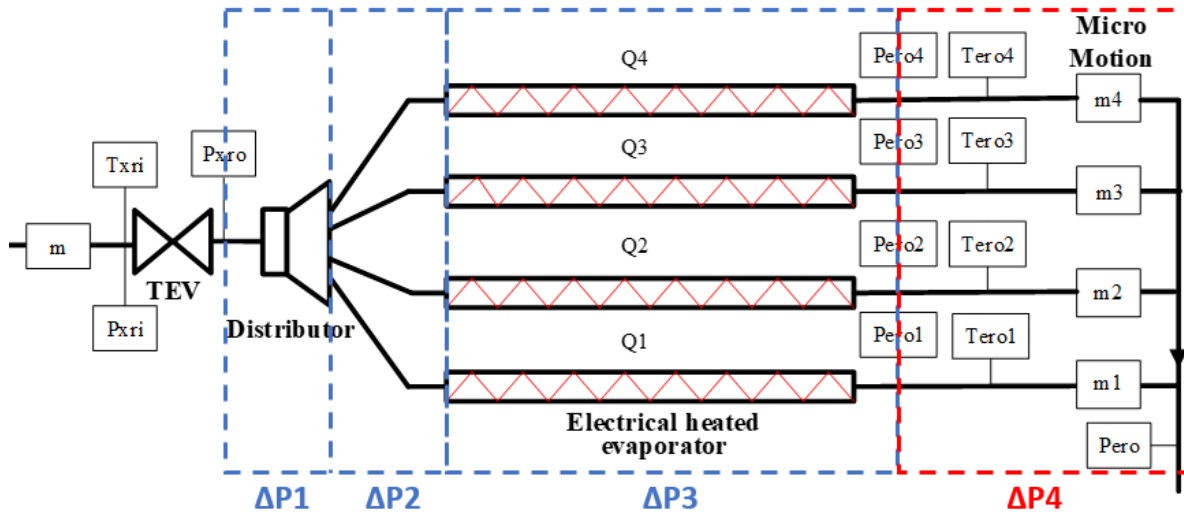


Figure 24 Schematic of pressure drop partition for each component

Pressure drop through distributor is assumed to be the same for all circuits. And pressure drop through evaporator is negligible because the cross-sectional area of evaporator is much larger than the feeder tubes. Based on calculation, pressure drop in evaporator is less than 0.5% of the pressure drop through feeder tubes. Thus, the pressure drop difference among each circuit is mainly happened in feeder tube (ΔP_2) and vapor phase (ΔP_4).

Refrigerant in feeder tubes is adiabatic two-phase flow. Compared to frictional pressure drop, acceleration pressure drop and gravitational pressure drop are negligible. Since tube length and material are same for each circuit, the difference in pressure drop is mainly caused by mass flow rate and quality. In Figure 25, the solid lines show the friction pressure drop as a function of mass flow rate and quality base on Friedel's correlation [29] and the dots represent the corresponding mass flow rate and quality of each circuit for one of the working conditions. In general, Friedel's correlation indicates that larger mass flow rate or higher quality would result in larger pressure drop. For this specific working condition, circuits with higher quality at distributor outlet (circuits 2 and 3) have larger pressure drop, and their mass flow rate are smaller than the other circuits. Similar conclusions can be obtained for other working conditions as shown in appendix A.

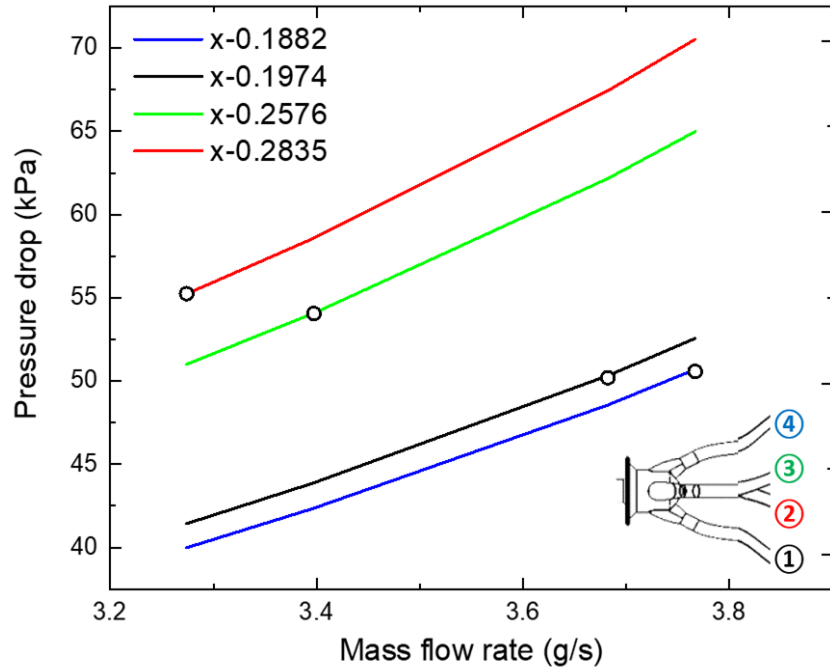


Figure 25 Adiabatic two-phase flow pressure drop as a function of mass flow rate and quality (horizontal, $m=15$ g/s, $x=0.22$)

Figure 26 shows the vapor phase pressure drop through Micro Motion and copper tubes (ΔP_4) as a function of mass flow rate for each circuit under three working conditions. It is nearly a linear relationship between pressure drop and mass flow rate, which means the circuit with higher mass flow rate will have larger pressure drop in superheated vapor phase.

From chapter 3, it has been concluded that for this distributor, some circuits always get higher mass flow rate and lower quality regardless of the working conditions. Combining the results from Figure 25 and Figure 26, circuits with higher mass flow rate usually have larger pressure drop in superheated vapor phase (ΔP_4) and lower pressure drop in two-phase (ΔP_2). Therefore, the larger pressure drop due to Micro Motion at downstream of evaporator can restrict refrigerant to the circuits with higher mass flow rate. That explains why the existence of Micro Motion can improve distribution as shown by Figure 22 and Figure 23.

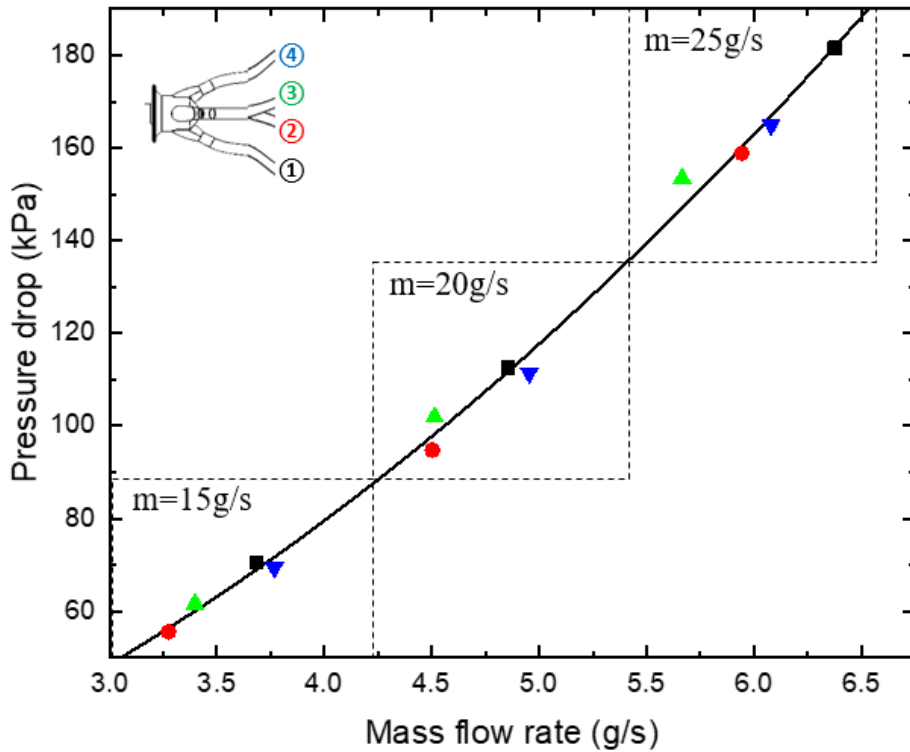


Figure 26 Pressure drop (ΔP_4) as a function of mass flow rate

4.2 Uniform heat load vs. uniform superheat

Different from real evaporator which provides cooling capacity to air flow, electrical heaters were used to absorb the latent heat of refrigerant from evaporator in this study. Superheat at the exits of evaporator was controlled to be the same for each circuit by adjusting heating power of the electrical heaters, which was how the experiments were conducted for the previous chapter. Another way to operate the system is providing uniform heat load to each circuit and evaluating the distribution of superheat.

Real evaporator works somewhere between these two extreme cases. To be more specific, if one of the circuits gets low mass flow rate, it will have lower capacity as is the case of uniform superheat, on the other hand, it will have higher superheat at evaporator exit as is the case with uniform heat load. The capacity of real evaporator is decided by the mutual effect of air flow and

refrigerant, which is difficult to be exactly simulated by the evaporator in this study. Instead, two extreme cases were examined.

Figure 27 shows the distribution of mass flow rate and superheat when same amounts of heat load were provided to all the circuits. In general, distribution of mass flow rate is much more uniform compared to superheat. For all the three working conditions, one of the circuits still has liquid at the exit of evaporator, while another circuit has superheat as high as 20 to 25 °C, which indicates an imperfect distribution of refrigerant in distributor. Compared to circuits 2 and 3, circuits 1 and 4 have higher mass flow rate and lower superheat. This is similar with what have been found when the evaporator was operated with uniform superheat. In short, the imperfect distribution happens with a similar pattern for both of the cases.

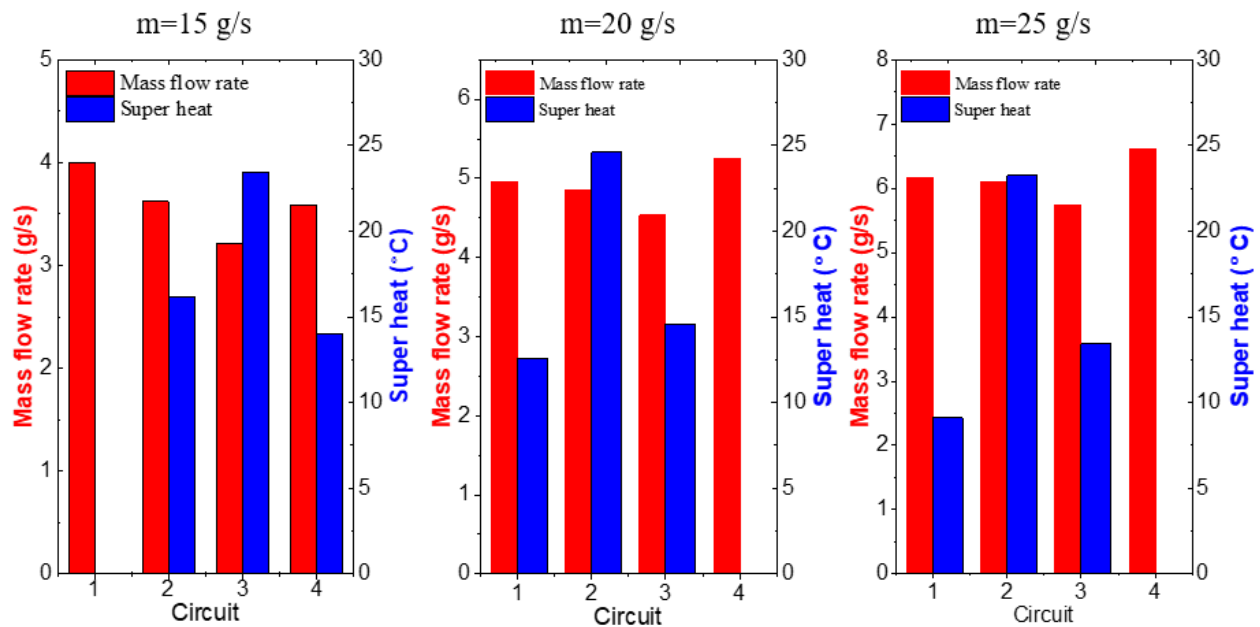


Figure 27 Distribution of mass flow rate and superheat (vertical upwards, $x=0.22$)

To compare refrigerant distribution under these two cases quantitatively, standard deviations of mass flow rate and quality are calculated and shown in Figure 28. The standard deviations of mass flow rate are almost the same for the cases of uniform heat load and uniform superheat, but the standard deviations of quality are different. Under the situation of uniform heat load, distribution of quality

is worse. It is expected that when this distributor is used in system with real evaporator, its performance would be between these two cases.

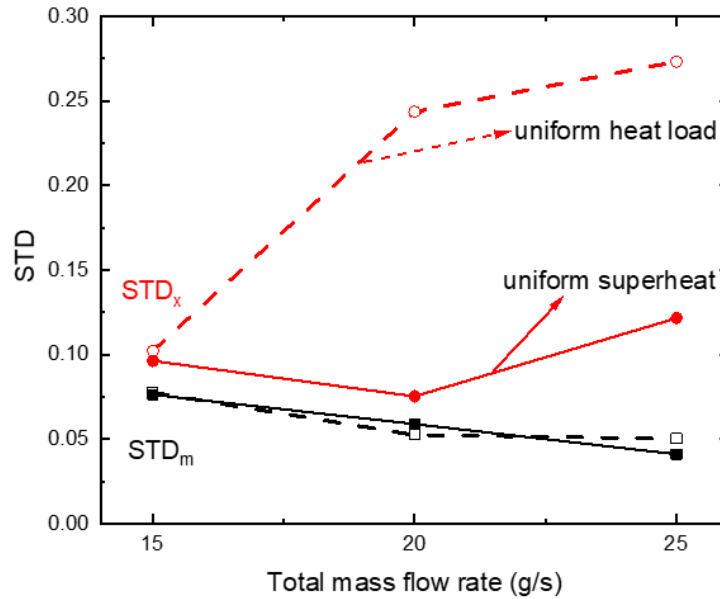


Figure 28 Standard deviation of mass flow rate and quality (vertical upwards, $x=0.22$)

4.3 Degradation in capacity due to maldistribution

Distribution of refrigerant mass flow rate and quality has been quantitatively analyzed in terms of standard deviation. In real application, the direct impact of refrigerant maldistribution on air conditioning system is the degradation in capacity. To create a baseline, four needle valves were installed downstream of the evaporator and before Micro Motions so that mass flow rate of each circuit can be controlled manually until uniform mass flow rate was achieved. Combining with the other two cases as discussed in section 4.2, the system has been operated under three different modes:

- Uniform mass flow rate

Keep $m_1=m_2=m_3=m_4$ by controlling needle valves in each circuit. But due to the maldistribution of quality, heat load needed by each circuit is not the same to achieve the same superheat.

- Uniform superheat
Keep $T_{ero1}=T_{ero2}=T_{ero3}=T_{ero4}$ by providing different heat load to each circuit.
- Uniform heat load
keep $Q_1=Q_2=Q_3=Q_4$ by controlling variacs, but superheat is different for each circuit due to refrigerant maldistribution

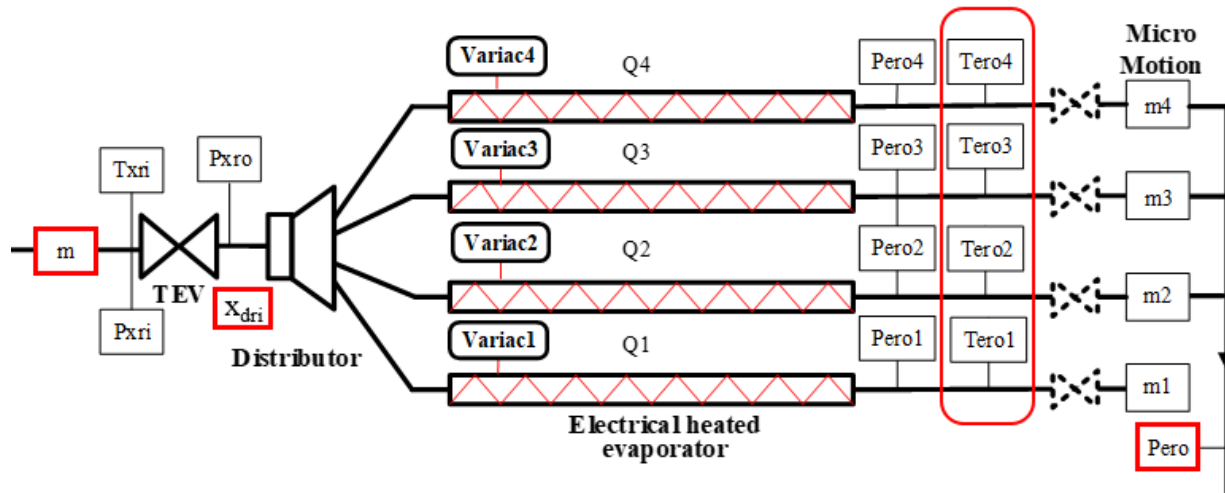


Figure 29 Demonstration of key parameters controlled as constant under three operating modes

To compare cooling capacity under different operating modes fairly, some parameters were controlled to be constant, including total mass flow rate, distributor inlet quality, compressor inlet pressure, and the average temperature at evaporator exits as demonstrated in Figure 29. Experiments results are shown in Figure 30 for the three operating modes. When uniform mass flow rate is achieved, distribution of quality is still imperfect. This is because external pressure from needle valves is applied to some of the circuits. If the uniform mass flow rate is achieved by distributor itself, according to the pressure drop analysis, distribution of quality should also be uniform. Compared to the results in the case of uniform superheat, distribution of heat load is better when mass flow rate is uniform because the difference in heat load is only caused by non-uniform quality. Under the situation of uniform heat load, there is a big difference in superheat distribution. Circuit 2 has a much larger superheat than all the other circuits, while circuit 4 has liquid refrigerant at the exit of evaporator. A similarity among the three operating modes is that circuit 2 always has the highest quality for all the working conditions. It needs a great effort to compensate for this

maldistribution. Because when needle valves were used to achieve uniform mass flow rate, valves for all the circuits except circuit 2 were tightened by several turns.

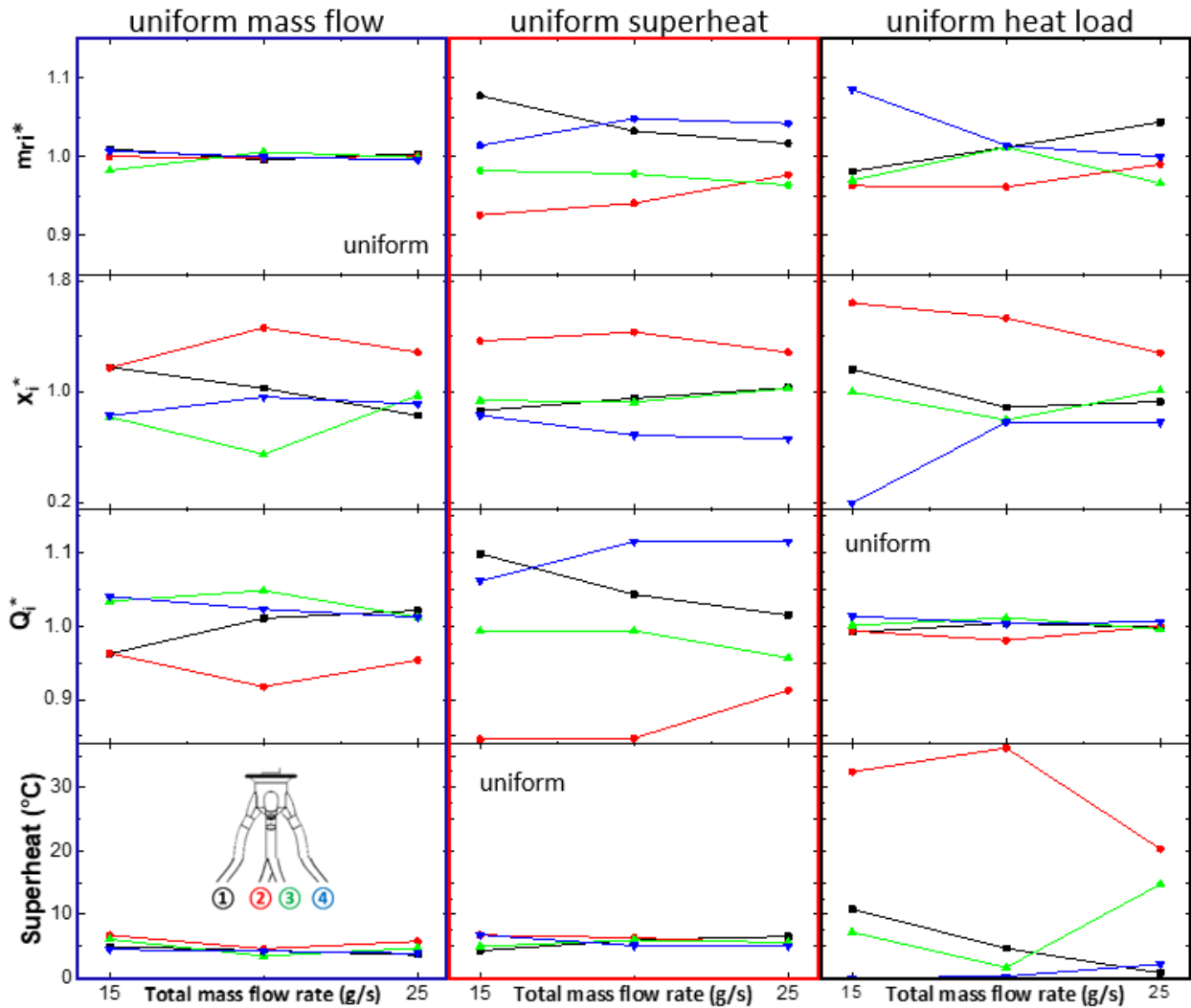


Figure 30 Distribution of mass flow rate, quality, heat load and superheat under three operating modes ($x=0.22$, vertical downwards)

Figure 31 compares the capacity ratio under three operating modes. Cooling capacity in the case of uniform mass flow rate is chosen as reference (100%), which is quite close with the capacity under the operating mode of uniform superheat. For these two cases, all the latent heat of refrigerant is absorbed by electrical heater and only vapor phase refrigerant leaves evaporator.

However, when the system is operated with uniform heat load, capacity is reduced by 2% to 5%. Because in this case, one of the circuits has two-phase flow at evaporator exit, that is a waste of potential cooling capacity. As the mass flow rate increases, degradation in capacity decreases because of the improvement in refrigerant distribution. In real application, both the maldistribution of refrigerant and air flow should be considered. If circuits with high refrigerant flow rate are matched with high air flow rate, it can compensate for the maldistribution. However, if the opposite situation is true, the maldistribution will get even worse.

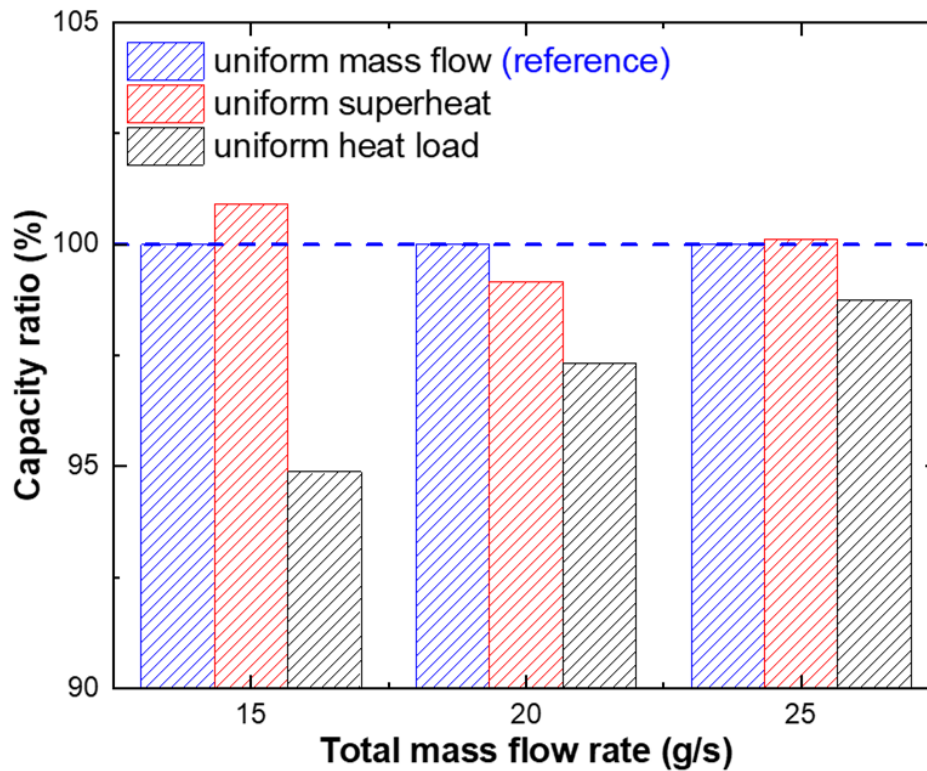


Figure 31 Capacity ratio under three operating modes

CHAPTER 5 VISUALIZATION

5.1 Representativeness of the transparent distributor

A transparent distributor was built based on the geometry of a commercial distributor from Parker Hannifin for the purpose of visualization. It is necessary to make sure that the performance of the transparent distributor can represent the original distributor. To achieve this object, both distributors have been tested under the same working conditions in our facility.

The original distributor is connected to the expansion valve by thread. When it is tightened properly, two of the circuits are located at the bottom and the other two are at the top, as show in Figure 32. For the transparent distributor, it was built with one of the circuits at bottom, two of them at middle, and the last one at the top.

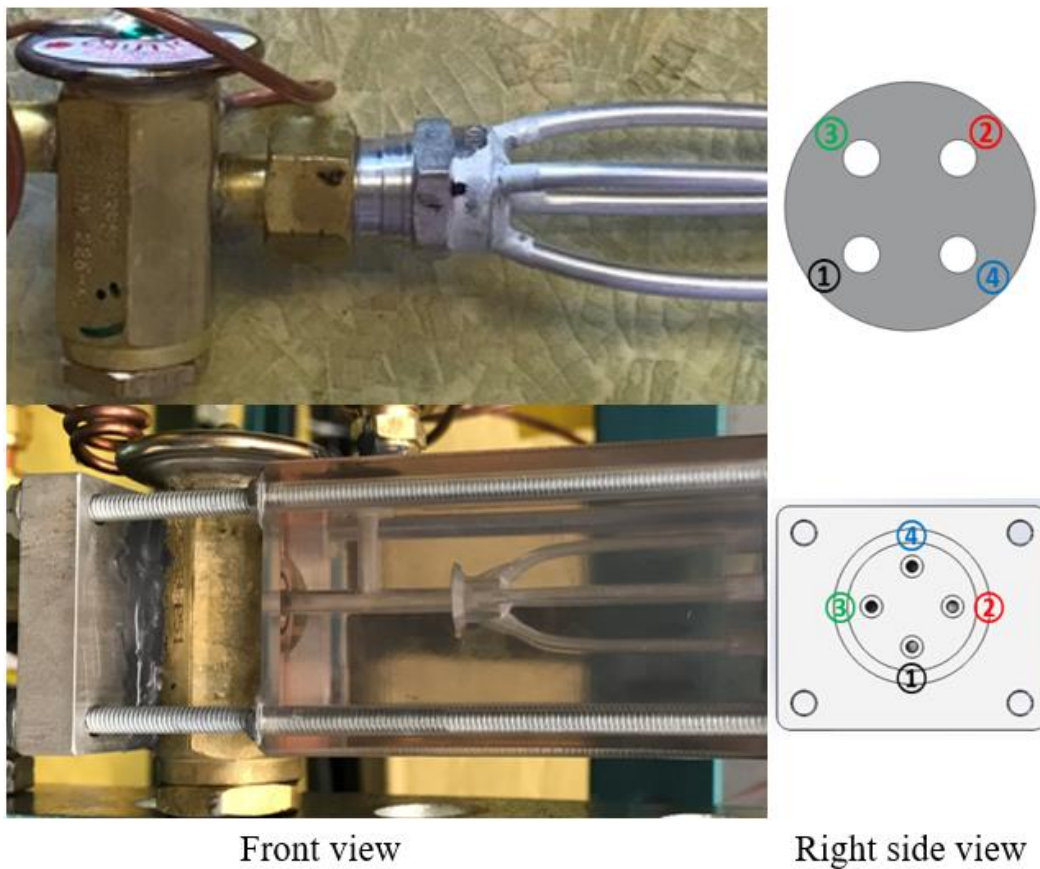


Figure 32 Location of circuits for original and transparent distributor

Figure 33 compares the distribution of non-dimensional heat load of the transparent and the original distributors at horizontal orientation. Lines with four different colors represent different circuits, and dash lines and solid lines mean original and transparent distributor respectively. Even locations of each circuit are not the same for these two distributors, the distribution of heat load shows a similar pattern. And if all the circuits are marked with numbers as shown in Figure 33, the resemblance of each circuit can also be observed. When both distributors are installed vertically, similar behavior happened again (see attached information in appendix C). This indicates that the transparent distributor can represent the original version very well.

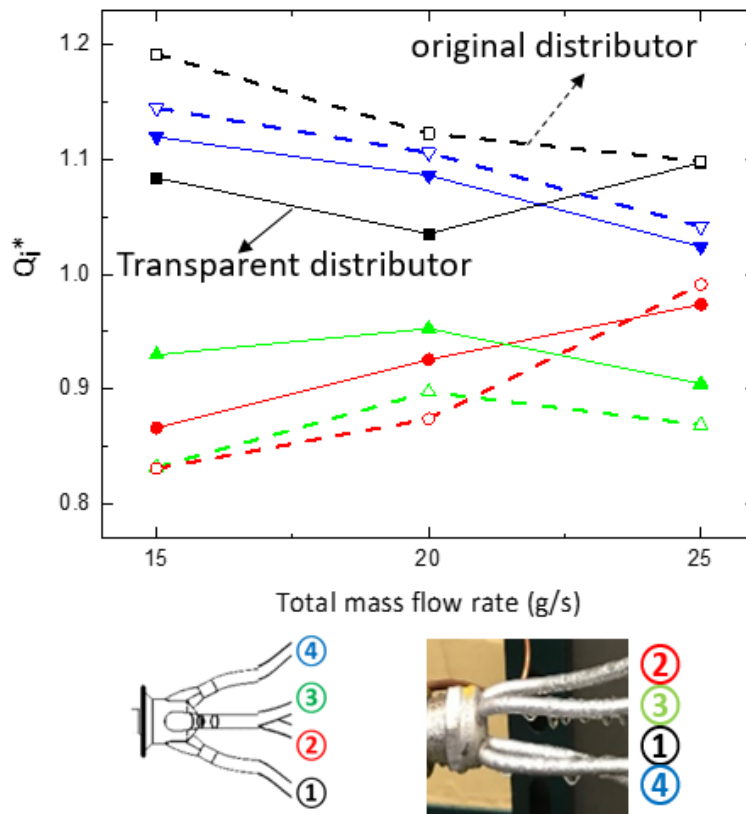


Figure 33 Distribution of non-dimensional heat load: original distributor vs. transparent distributor (horizontal, $x=0.22$)

5.2 Visualization of refrigerant two-phase flow in distributor

Maldistribution of refrigerant two-phase flow in distributor has been quantified by experiments as discussed in the previous chapters. To understand what is happening inside of the distributor, visualization by high-speed camera is a good option.

Asano et al. [30] visualized refrigerant two-phase flow in a reservoir type distributor by neutron radiography and a high sensitivity video camera was used. A liquid pool was observed at the bottom of the distributor with a turbulent interface and part of the liquid was dragged up by the incoming two-phase flow. A similar result was found by Yoshioka et al. [9] who also visualized refrigerant two-phase flow in a reservoir distributor made of poly-carbonate resin. It was found that maldistribution of refrigerant two-phase flow can be attributed to the inclination of the incoming flow. Aziz et al. [31] visualized air and water two-phase flow in a distributor made of acrylic resin. It indicated that at horizontal orientation, uniform distribution can be achieved when superficial velocity for both air and water is very high. Other than distributors, two-phase flow visualization has been even more widely used in headers as a way to study the flow behaviors. Representative references are listed in [32-40].

A transparent distributor made of WaterClear Ultra was built by 3D printing for this study. Two-phase flow exiting expansion valve and through distributor until the entrance of the evaporator can be visualized by high speed camera. Figure 34 shows the two-phase flow in distributor and the inlet tube at horizontal orientation. At low mass flow rate, it is clearly annular flow in the inlet tubes. And liquid film at the bottom of the tube is a little thicker than that at the top. Accordingly, vapor phase refrigerant is observed at the middle of the distributor and surrounded by liquid at top and bottom. As mass flow rate increases gradually, the vapor core at the center of the inlet tube is becoming less obvious and vapor phase refrigerant is not concentrated at a certain part of the distributor any more. As discussed in Chapter 3, when mass flow rate is between 15 to 25 g/s, (mass flux is between 1215 to 2125 kg/m²s in the inlet tube and 350 to 620 kg/m²s in distributor) refrigerant distribution is not influenced by gravity. This is verified by the visualization results, because flow in this range of mass flow rate is not a typical annular flow but approaching to homogeneous.

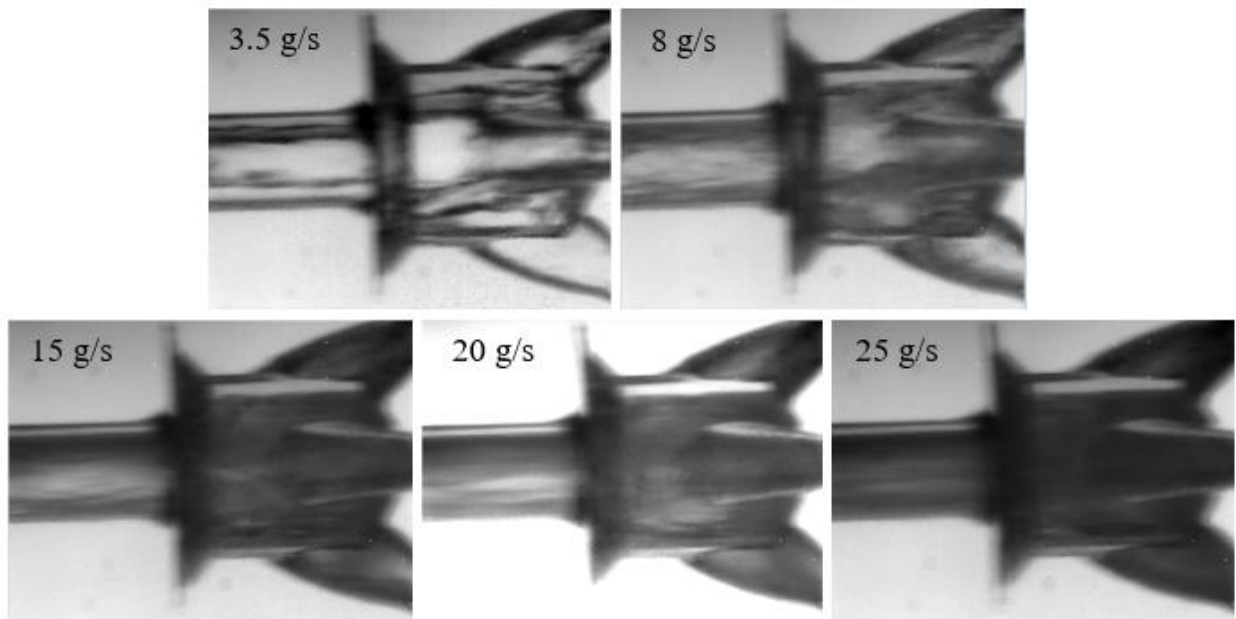


Figure 34 Visualization of two-phase flow in distributor and the inlet tube (horizontal)

The visualization results also reveal how the flow behaves inside distributor. When mass flow rate is between 15 to 25 g/s, the main flow from inlet tube will reach the sharp base of the distributor directly and then recirculate around the mainstream. The recirculating flow will then distribute into each circuit. A similar pattern has been observed by Li et al. [16] through simulation, as shown in Figure 35. A distributor with similar structure was used, and the contours of velocity vector reflect what was observed in this study. But when mass flow rate is low (3.5 and 8 g/s), recirculation does not happen. Instead, refrigerant around the mainstream stays relatively still because of the low velocity. Consequently, refrigerant distribution is expected to be bad in these situations.

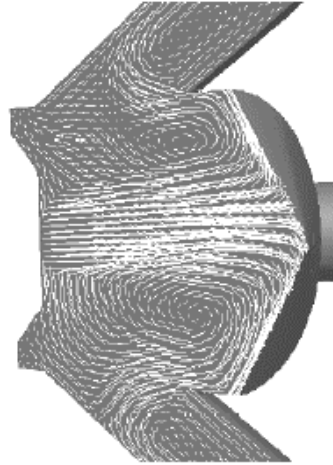


Figure 35 Velocity vector contours in distributor [16]

When distributor is installed vertically, the flow pattern is similar with the results at horizontal orientation, as shown in Figure 36 and Figure 37. Annular flow is observed at the inlet tube when mass flow rate is low. And the flow inside distributor is also kind of annular because vapor phase is mainly observed at the center of distributor. When mass flow rate is increased, the two-phase flow changes from annular to a more homogeneous pattern. The similarity in flow pattern between horizontal and vertical orientation is reasonable, because the distribution of mass flow rate and heat load is almost the same regardless of orientation.

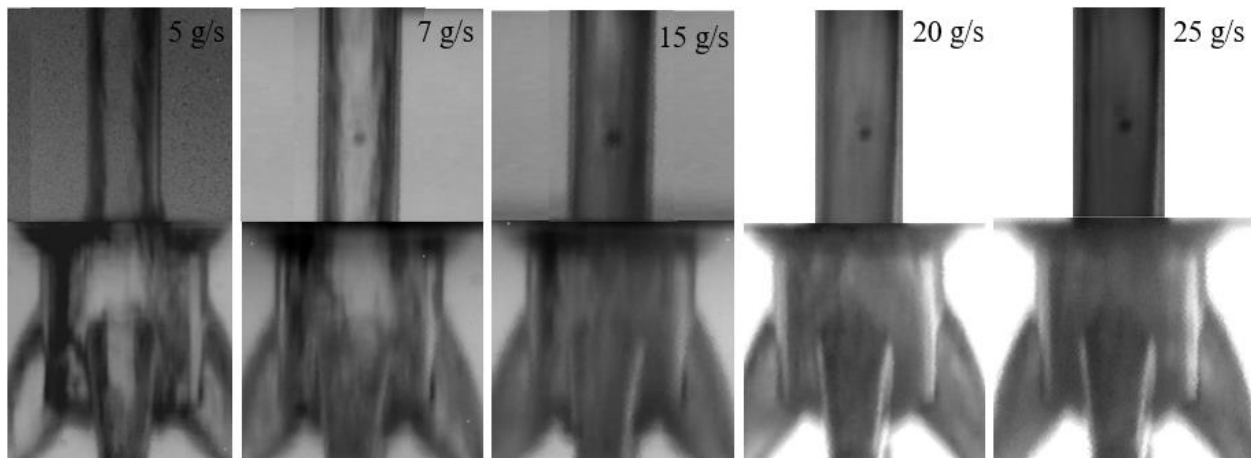


Figure 36 Visualization of two-phase flow in distributor and the inlet tube (vertical downward)

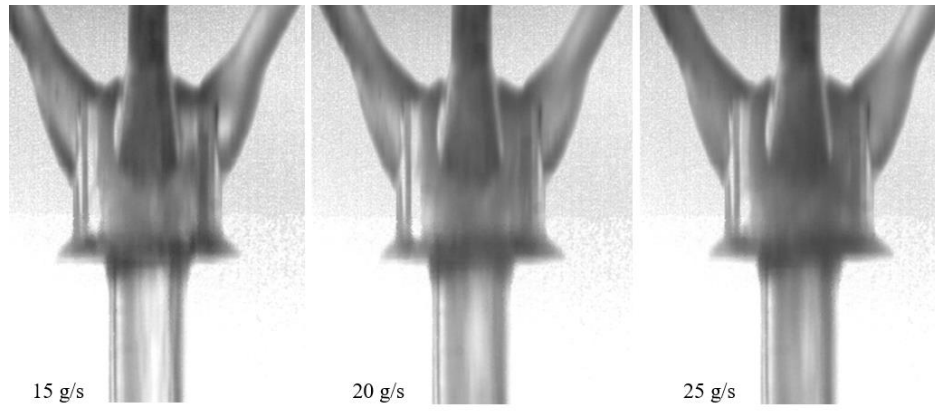


Figure 37 Visualization of two-phase flow in distributor and the inlet tube (vertical upward)

CHAPTER 6 CONCLUSION

6.1 Summary

This study investigated several possible factors influencing the performance of refrigerant distributor such as mass flow rate, distributor inlet quality and orientation in an air conditioning system using R134a as working fluid. Although the experiment facility is quite close to a real AC system, it is inevitable to have some deviation for the purpose of measurement. Effects of these differences from real system were analyzed. In addition, two-phase flow in distributor as well as the inlet tube was visualized by high-speed camera to understand the flow behavior. The main conclusions are as follows:

- Distribution of mass flow rate and quality show a similar pattern under different working conditions, in other words, some circuits always get more refrigerant than others.
- The performance of distributor is improved as mass flow rate increases because high velocity can result in more homogeneous flow.
- Lower distributor inlet quality also improves distribution. A possible explanation is that flow is closer to single phase as the percent of vapor phase decreased.
- Orientation has no effect on distribution, which indicates that two-phase flow does not separate in distributor.
- The existence of Micro Motion at downstream of evaporator improves the distribution to some degree. That is to say the performance of this distributor will be a little worse in a real system than estimated in this study.
- When different heat loads were provided to achieve the same superheat at the evaporator exits, the cooling capacity is larger than the situation with uniform heat load. Because for the first case, all the liquid phase refrigerant was fully utilized. However, the distribution of mass flow rate and quality have a similar pattern for these two cases.
- Visualization results show that it is annular flow at the inlet of distributor when refrigerant mass flow rate is extremely low. As the mass flow rate increases gradually, the flow is approaching to a more homogeneous state, and the distribution was improved accordingly.

6.2 Future work

This study mainly focused on the performance of refrigerant distributor. However, according to the visualization results, flow regime between expansion valve and distributor plays an important role in two-phase distribution. Bowers [32] has studied flow development after expansion device in a system without oil and briefly mentioned the effect of oil on flow regime. It seems that the existence of oil will change the flow regime and flow development dramatically. So, the future work will look into the effect of flow regimes in straight tube including L and U bends on flow development characteristics in adiabatic two-phase flow after an expansion device to help improving distribution, design of distributors, and inlet headers in the case of parallel flow evaporators. The effect of oil on flow regime and distribution will be taken into account, as is the case with real system.

REFERENCES

1. *Venturi-Flo Low Pressure Drop Distributors - Products control devices*. 2017. Available from: <http://www.cdvalve.com/products/detail/venturi-flotrade-low-pressure-drop-distributors>
2. *Distributors and flow controls-Parker Hannifin Corporation*. 2007. Available from: <https://www.parker.com/literature/Sporlan/Climate%20Systems%20Literature/PDF%20files/CatalogOEM-3.pdf>
3. Fay, M.A., *Effect of conical distributors on evaporator and system performance*. 2012. (Master Thesis) University of Illinois at Urbana-Champaign.
4. Chen, S.S., *Refrigerant distribution model development*. 1995, Massachusetts Institute of Technology.
5. Nakayama, M., et al., *Development of a refrigerant two-phase flow distributor for a room air conditioner*. 2000. International Refrigeration and Air Conditioning Conference. Paper 497.
6. Liang, J., et al., *EXPERIMENTAL INVESTIGATION ON PERFORMANCE OF A NEW TYPE OF DISTRIBUTOR [J]*. Refrigeration and Air Conditioning, 2004. **2**: p. 006.
7. Wen, M.-Y., C.-H. Lee, and J.-C. Tasi, *Improving two-phase refrigerant distribution in the manifold of the refrigeration system*. Applied Thermal Engineering, 2008. **28**(17-18): p. 2126-2135.
8. Bowers, C.D., et al., *Improvements in Refrigerant Flow Distribution Using an Expansion Valve with Integrated Distributor*. 2014. International Refrigeration and Air Conditioning Conference. Paper 1458.
9. Yoshioka, S., H. Kim, and K. Kasai, *Performance Evaluation and Optimization of A Refrigerant Distributor for Air Conditioner*. Journal of Thermal Science and Technology, 2008. **3**(1): p. 68-77.
10. Zhang, C., Y. Wang, and J. Chen, *Optimization of the Reserve-Type Distributor for R410a Air Conditioner*. International Journal of Air-Conditioning and Refrigeration, 2014. **22**(04).
11. Han, Q., C. Zhang, and J. Chen, *EXPERIMENTAL AND CFD INVESTIGATION OF R410A DISTRIBUTORS FOR AIR CONDITIONER*. International Journal of Air-Conditioning and Refrigeration, 2014. **22**(2): p. 1-11.
12. Zhang, C., et al., *Experimental and Numerical Investigations of the Double-Barrel Distributor for Air Conditioner*. International Journal of Air-Conditioning and Refrigeration, 2015. **23**(03).
13. Wang, D., et al., *Influence factors of flow distribution and a feeder tube compensation method in multi-circuit evaporators*. International Journal of Refrigeration, 2017. **73**: p. 11-23.
14. Choi, J.M., W.V. Payne, and P.A. Domanski. *Effects of non-uniform refrigerant and air flow distributions on finned-tube evaporator performance*. in *International Congress Refrigeration*. 2003.
15. Liang, F., et al., *Gas-liquid two-phase flow equal distribution using a wheel distributor*. Experimental Thermal and Fluid Science, 2014. **55**: p. 181-186.
16. Li, G., et al., *Evaluating the performance of refrigerant flow distributors*. 2002. International Refrigeration and Air Conditioning Conference. Paper 593.

17. Li, G., et al., *Application of CFD models to two-phase flow in refrigerant distributors*. HVAC&R Research, 2005. **11**(1): p. 45-62.
18. Ishii, E. and K. YOSHIMURA, *Gas-Liquid Flow Simulation in Refrigerant Distributor for Air Conditioner*. International Journal of Air-Conditioning and Refrigeration, 2013. **21**(03): p. 1350017.
19. Ishikawa, M., E. Ishii, and M. Ikegawa. *Simulation of Gas-Liquid Free Surface Flows in a Refrigerant Distributor and a Nozzle of Continuous-Inkjet*. in *ASME 2013 International Mechanical Engineering Congress and Exposition*. 2013. American Society of Mechanical Engineers.
20. Li, G., et al., *Application Of CFD Models To Two-Phase Flow In Refrigerant Distributors*. 2002. International Refrigeration and Air Conditioning Conference. Paper 592.
21. Ishii, E., M. Ishikawa, and K. Yoshimura, *Numerical Approach to Study Nonuniform Gas-Liquid Distribution in the Refrigerant Distributor in an Air Conditioner*. Journal of Fluids Engineering, 2015. **137**(11): p. 111303.
22. Han, Q., *Study on the performance of refrigerant distributor*. 2014, Shanghaijiaotong University.
23. Kærn, M.R. and B. Elmegaard, *Analysis of refrigerant mal-distribution in fin-and-tube evaporators*. Danske Kølledage, 2009. **2009**: p. 25-35.
24. Kærn, M.R., et al., *Performance of residential air-conditioning systems with flow maldistribution in fin-and-tube evaporators*. International Journal of Refrigeration, 2011. **34**(3): p. 696-706.
25. Kærn, M.R., et al., *Compensation of flow maldistribution in fin-and-tube evaporators for residential air-conditioning*. international journal of refrigeration, 2011. **34**(5): p. 1230-1237.
26. Kim, J.-H., J.E. Braun, and E.A. Groll, *A hybrid method for refrigerant flow balancing in multi-circuit evaporators: Upstream versus downstream flow control*. international journal of refrigeration, 2009. **32**(6): p. 1271-1282.
27. Kim, J.-H., J.E. Braun, and E.A. Groll, *Evaluation of a hybrid method for refrigerant flow balancing in multi-circuit evaporators*. international journal of refrigeration, 2009. **32**(6): p. 1283-1292.
28. Heikal, R., *Study of Flow Maldistribution inside an Air Conditioning Distributor Using FLUENT Simulation*. Applied Mechanics and Materials, 2015. **799-800**: p. 712-719.
29. Friedel, L., *Improved friction pressure drop correlation for horizontal and vertical two-phase pipe flow*. Proc. of European Two-Phase Flow Group Meet., Ispra, Italy, 1979.
30. Asano, H., et al., *Visualization and measurement of refrigerant flow in compression-type refrigerator by neutron radiography*. Nuclear Instruments and Methods in Physics Research Section A: Accelerators, Spectrometers, Detectors and Associated Equipment, 1999. **424**(1): p. 98-103.
31. Aziz, A., A. Miyara, and F. Sugino, *Distribution of two-phase flow in a distributor*. J. Eng. Sci. Technol, 2012. **7**(1): p. 41-55.
32. Lee, Jun Young. "Optimum channel intrusion depth for uniform flow distribution at header-channel junctions." Journal of mechanical science and technology 24, no. 7 (2010): 1411-1416.
33. Byun, H. W., and N. H. Kim. "Refrigerant distribution in a parallel flow heat exchanger having vertical headers and heated horizontal tubes." Experimental Thermal and Fluid Science 35, no. 6 (2011): 920-932.

34. Kim, Nae-Hyun, Ho-Won Byun, and Yong-Sub Sim. "Upward branching of two-phase refrigerant in a parallel flow minichannel heat exchanger." *Experimental Thermal and Fluid Science* 51 (2013): 189-203.
35. Zou, Yang, and Pega S. Hrnjak. "Experiment and visualization on R134a upward flow in the vertical header of microchannel heat exchanger and its effect on distribution." *International Journal of Heat and Mass Transfer* 62 (2013): 124-134.
36. Li, Jun, and Predrag Hrnjak. Phase Separation in Second Header of MAC Condenser. No. 2015-01-1694. SAE Technical Paper, 2015.
37. Li, Jun, and Predrag Hrnjak. The Analysis of Phase Separation in Vertical Headers of Microchannel HEs. No. 2016-01-0253. SAE Technical Paper, 2016.
38. Marchitto, Annalisa, Marco Fossa, and Giovanni Guglielmini. "Phase split in parallel vertical channels in presence of a variable depth protrusion header." *Experimental Thermal and Fluid Science* 74 (2016): 257-264.
39. Li, Jun, and Pega Hrnjak. "Visualization and quantification of separation of liquid-vapor two-phase flow in a vertical header at low inlet quality." *International Journal of Refrigeration* 85 (2018): 144-156.
40. Li, Jun, and Pega Hrnjak. "Phase Separation in Vertical Header of Microchannel Condensers: A Mechanistic Model." In *ASME 2018 5th Joint US-European Fluids Engineering Division Summer Meeting*, pp. V003T20A003. American Society of Mechanical Engineers, 2018.
41. Bowers, C.D., *Developing adiabatic two-phase flow*. 2009: University of Illinois at Urbana-Champaign.

APPENDIX A PRESSURE DROP IN FEEDER TUBE

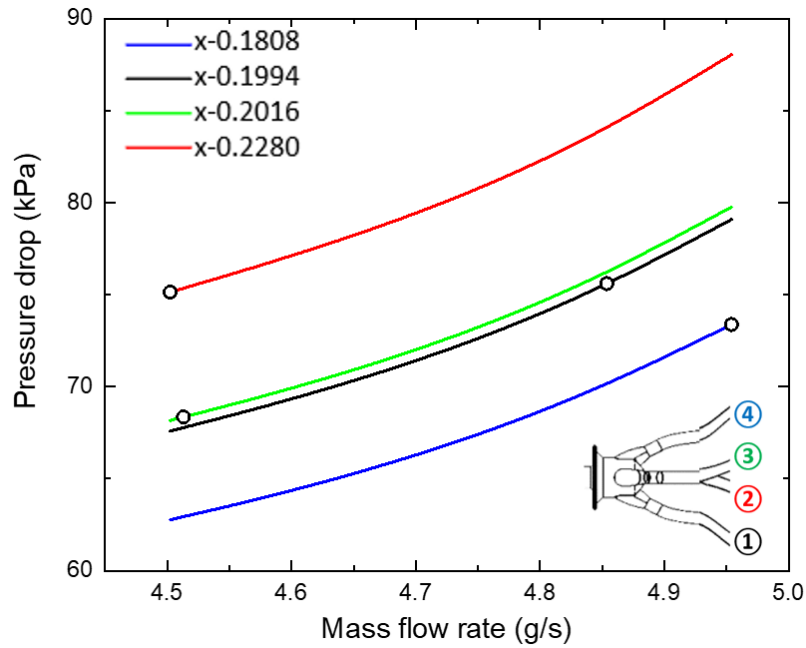


Figure 38 Adiabatic two-phase flow pressure drop as a function of mass flow rate and quality (horizontal, $m=20$ g/s, $x=0.22$)

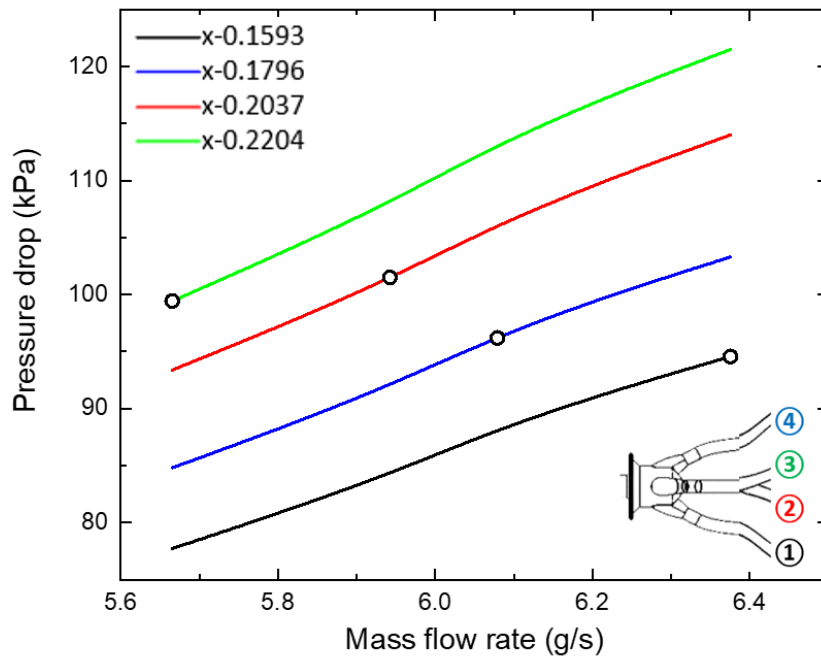


Figure 39 Adiabatic two-phase flow pressure drop as a function of mass flow rate and quality (horizontal, $m=25$ g/s, $x=0.22$)

APPENDIX B CALCULATED PRESSURE DROP VS. MEASURED PRESSURE DROP

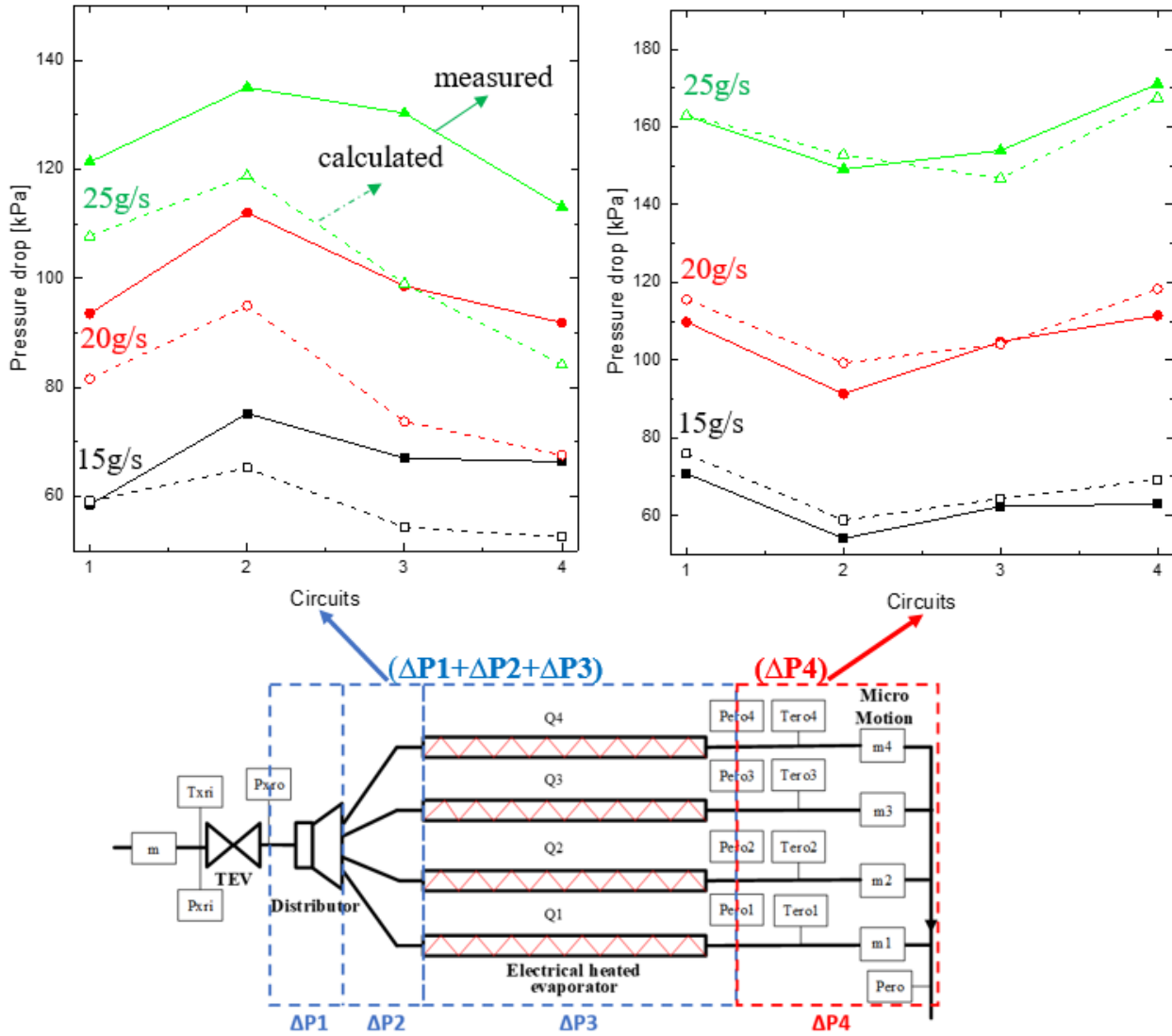


Figure 40 Comparison of pressure drop between calculated and measured values

APPENDIX C REPRESENTATIVENESS OF THE TRANSPARENT DISTRIBUTOR

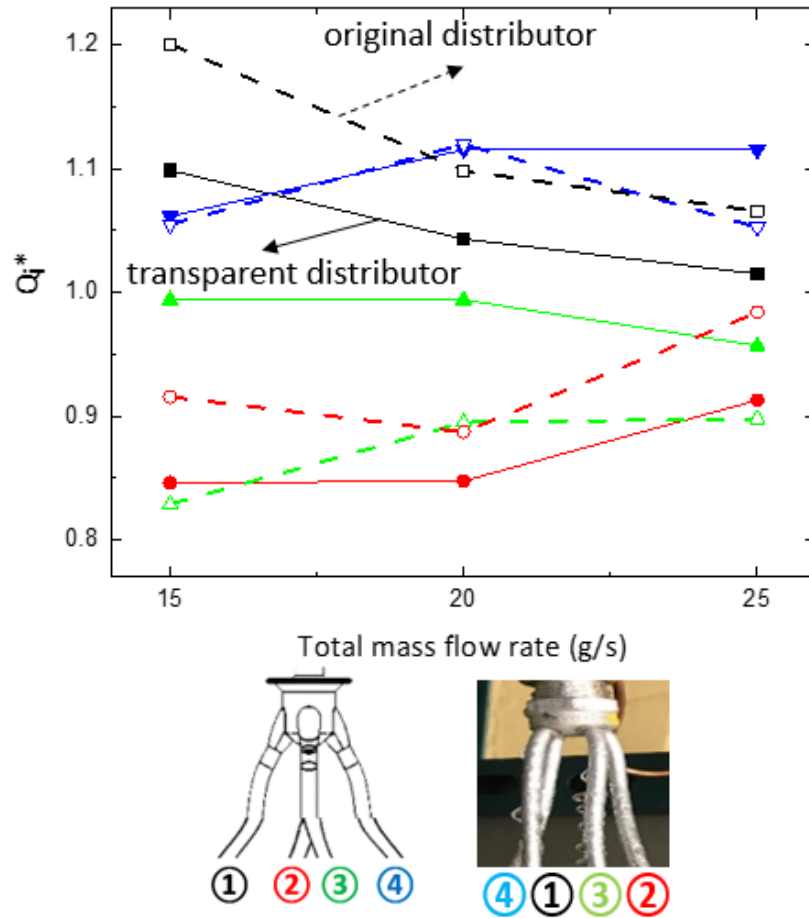


Figure 41 Distribution of non-dimensional heat load: original distributor vs. transparent distributor (vertical downward, $x=0.22$)

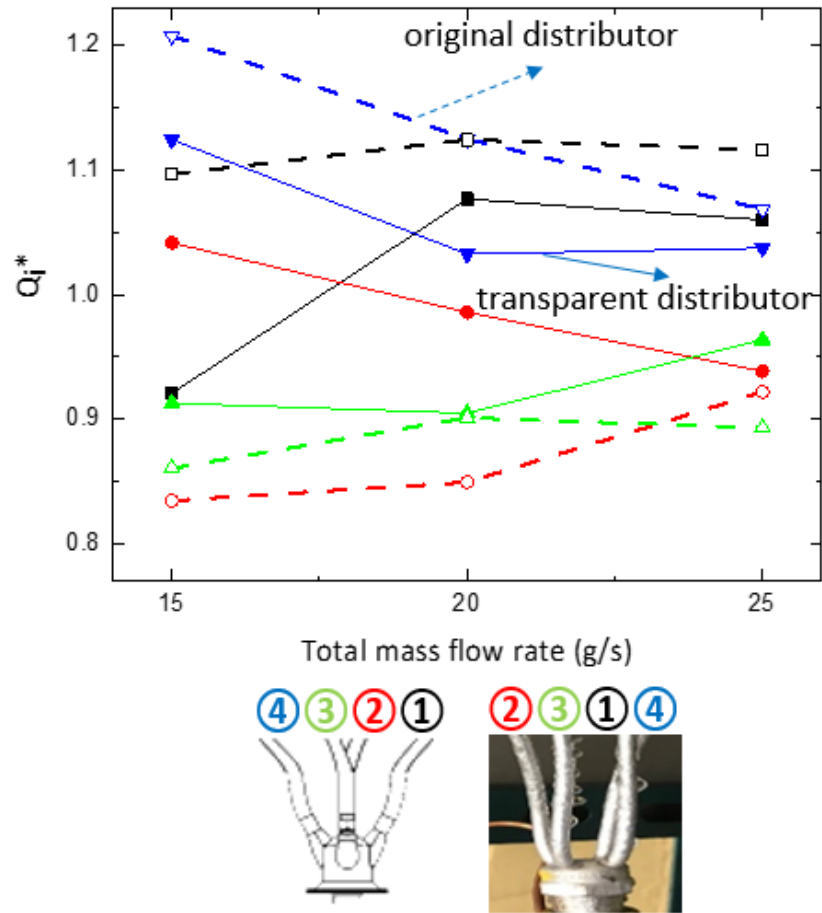


Figure 42 Distribution of non-dimensional heat load: original distributor vs. transparent distributor (vertical upward, $x=0.22$)

APPENDIX D ORIGINAL DATA

Table 5 Experiment results under five working conditions at vertical upward orientation

Working conditions	Pressure [kPa]						
	P _{xri}	P _{dri}	P _{ero1}	P _{ero2}	P _{ero3}	P _{ero4}	P _{ero}
1	1442.985	516.1281	439.2056	439.0234	433.8776	447.447	385.3771
2	1465.968	601.4576	501.7117	486.2614	478.8385	493.5885	375.0443
3	1461.834	692.1789	560.7321	535.0084	537.381	552.8681	375.0896
4	1455.81	644.2211	552.0674	525.3367	552.4155	549.3449	380.5918
5	1460.941	615.1711	550.526	530.7641	550.9162	550.2442	384.1812
Working conditions	Temperature [°C]						
	T _{xri}	T _{ero1}	T _{ero2}	T _{ero3}	T _{ero4}	T _{ref}	
1	44.76235	19.75431	20.33339	20.23777	21.22096	29.58302	
2	47.48902	26.4123	25.83284	24.35898	26.74783	30.77232	
3	49.26625	28.21003	27.46222	28.29933	28.31583	32.98008	
4	39.21478	25.42353	24.80837	25.88787	24.69178	29.31158	
5	31.12477	28.46387	26.75602	26.55728	27.42813	30.2052	
Working conditions	Mass flow rate [g/s]						
	m ₁	m ₂	m ₃	m ₄	m		
1	3.45566	3.707961	3.171342	3.89291	14.61754		
2	5.042673	4.902464	4.335572	4.998566	19.45302		
3	6.455076	6.192708	5.812087	6.416939	24.94322		
4	6.014032	5.56024	5.904053	6.060355	24.55195		
5	5.973188	5.76437	5.928463	6.134718	24.91332		
Working conditions	Quality [-]						
	X _{eri1}	X _{eri2}	X _{eri3}	X _{eri4}	X _{xro}		
1	0.284113	0.246366	0.226671	0.225685	0.25336		
2	0.219995	0.268298	0.231791	0.24926	0.256728		
3	0.207454	0.272014	0.202759	0.221718	0.248565		
4	0.147122	0.171586	0.092708	0.1321	0.159608		
5	0.078057	0.103495	0.03043	0.068159	0.095653		
Working conditions	Heating power [W]						
	Q ₁	Q ₂	Q ₃	Q ₄			
1	495.6275	560.6809	491.3595	605.4298			
2	790.8249	723.9101	664.3733	758.3271			
3	1001.868	886.8826	910.8238	980.449			
4	978.0239	879.9557	1021.989	998.0096			
5	1065.386	994.9386	1098.584	1098.538			

Table 6 Experiment results under five working conditions at vertical downward orientation

Working conditions	Pressure [kPa]						
	P_{xri}	P_{dri}	P_{ero1}	P_{ero2}	P_{ero3}	P_{ero4}	P_{ero}
1	1446.902	515.5022	456.9994	440.2699	448.4777	449.1073	386.1563
2	1461.249	590.9212	497.3551	478.8713	492.3114	499.0313	387.556
3	1458.238	670.9173	549.5541	535.8722	540.6493	557.7974	386.7168
4	1463.867	645.3476	557.2861	552.6879	559.1974	558.2472	392.1295
5	1462.014	627.2165	567.7705	561.9906	568.181	564.3965	394.9225
Working conditions	Temperature [°C]						
	T_{xri}	T_{ero1}	T_{ero2}	T_{ero3}	T_{ero4}	T_{ero}	T_{ref}
1	43.2995	17.26876	18.57784	17.3452	19.20776	25.85185	32.14038
2	46.2273	21.55124	20.73401	21.2348	20.76913	28.80309	33.69051
3	47.79116	25.27747	23.42194	23.82163	24.23428	30.42059	34.57808
4	38.7308	24.62983	24.45644	23.75809	24.57516	30.76251	34.17244
5	31.98858	24.2123	23.11542	24.29856	23.55474	29.85609	32.89952
Working conditions	Mass flow rate [g/s]						
	m_1	m_2	m_3	m_4	m		
1	3.96672	3.407783	3.615904	3.734066	15.26399		
2	5.012374	4.567939	4.748031	5.088716	20.07288		
3	6.150969	5.908939	5.830954	6.303847	24.9964		
4	6.204635	6.158973	6.110693	6.213446	24.96716		
5	6.346112	6.255835	6.195656	6.256611	25.03581		
Working conditions	Quality [-]						
	X_{eri1}	X_{eri2}	X_{eri3}	X_{eri4}	X_{xro}		
1	0.176625	0.279698	0.191727	0.169478	0.235381		
2	0.182059	0.273325	0.176821	0.131049	0.240919		
3	0.189475	0.236329	0.188455	0.1212	0.2349		
4	0.119456	0.137426	0.089169	0.071525	0.15297		
5	0.06469	0.073939	0.028383	0.022212	0.095309		
Working conditions	Heating power [W]						
	Q_1	Q_2	Q_3	Q_4			
1	628.6365	484.0657	568.6697	607.3148			
2	793.0911	644.2874	755.6996	848.0515			
3	956.8993	860.4709	901.9965	1051.219			
4	1031.346	1004.055	1044.931	1085.77			
5	1110.016	1078.536	1125.903	1138.403			

Table 7 Experiment results under five working conditions at horizontal orientation

Working conditions	Pressure [kPa]						
	P_{xri}	P_{dri}	P_{ero1}	P_{ero2}	P_{ero3}	P_{ero4}	P_{ero}
1	1445.598	508.435	450.5561	435.5951	441.6546	449.4663	380.0511
2	1456.736	582.6512	494.0639	476.2229	483.4305	492.9105	381.5041
3	1456.104	672.3467	564.9645	542.2404	536.7864	548.3432	383.3707
4	1460.188	632.2394	548.5633	545.5815	550.793	542.8984	387.4074
5	1459.642	609.8249	551.9911	550.7294	552.8777	548.3778	386.848
Working conditions	Temperature [°C]						
	T_{xri}	T_{ero1}	T_{ero2}	T_{ero3}	T_{ero4}	T_{ero}	T_{ref}
1	41.59245	21.2502	20.75569	21.0055	21.09628	20.99258	26.32505
2	45.07297	23.76783	22.86262	22.14034	24.83547	26.55641	28.39277
3	47.09829	25.42194	25.24313	24.2164	25.31235	28.32469	30.08018
4	36.41074	23.64625	22.81811	24.02513	24.25335	28.59101	32.26469
5	29.71916	23.5567	23.1379	24.41548	24.49449	28.28983	31.25029
Working conditions	Mass flow rate [g/s]						
	m_1	m_2	m_3	m_4	m		
1	3.68228	3.273985	3.397397	3.766965	15.11043		
2	4.853691	4.502372	4.513052	4.953976	19.98724		
3	6.375651	5.942196	5.665258	6.079213	25.17014		
4	6.141811	6.158861	6.086233	6.0544	24.79308		
5	6.096827	6.1711	6.043998	6.094371	24.6717		
Working conditions	Quality [-]						
	X_{eri1}	X_{eri2}	X_{eri3}	X_{eri4}	X_{xro}		
1	0.197366	0.283508	0.25763	0.188162	0.224723		
2	0.19935	0.228025	0.201569	0.180783	0.235085		
3	0.159343	0.203692	0.220442	0.179638	0.230588		
4	0.112817	0.084653	0.079984	0.094022	0.137666		
5	0.050916	0.031324	0.034301	0.037158	0.083793		
Working conditions	Heating power [W]						
	Q_1	Q_2	Q_3	Q_4			
1	590.3607	471.5676	506.2962	609.7984			
2	766.7848	685.4968	705.528	804.565			
3	1028.15	912.203	847.2901	959.2172			
4	1028.055	1058.64	1057.733	1038.508			
5	1087.772	1121.193	1101.988	1108.541			

Table 8 Experiment results without Micro Motion under three working conditions at vertical downward orientation

Working conditions	Pressure [kPa]						
	P_{xri}	P_{dri}	P_{ero1}	P_{ero2}	P_{ero3}	P_{ero4}	P_{ero}
1	1444.90	513.60	452.40	444.21	449.76	453.79	415.69
2	1459.84	592.79	496.28	482.84	490.01	498.23	433.78
3	1458.46	672.26	544.78	528.10	531.54	535.05	447.07
Working conditions	Temperature [°C]						
	T_{xri}	T_{ero1}	T_{ero2}	T_{ero3}	T_{ero4}	T_{ero}	T_{ref}
1	42.90	20.03	21.04	20.14	21.83	29.10	31.76
2	46.38	20.51	19.74	21.54	21.13	29.32	32.87
3	47.84	24.83	22.59	23.77	23.44	30.85	34.06
Working conditions	Heating power [W]						
	Q_1	Q_2	Q_3	Q_4			
1	568.1358	424.87104	589.45449	658.475			
2	768.2987	613.56809	776.34612	882.3935			
3	1020.7976	864.20205	957.77198	979.3454			

Table 9 Experiment results with uniform heat load under three working conditions at vertical upward orientation

Working conditions	Pressure [kPa]						
	P_{xri}	P_{dri}	P_{ero1}	P_{ero2}	P_{ero3}	P_{ero4}	P_{ero}
1	1455.27	523.25	456.23	442.48	437.69	442.80	380.18
2	1469.68	607.48	497.97	487.38	490.58	501.47	378.51
3	1459.87	693.65	560.38	547.33	550.48	557.40	371.21
Working conditions	Temperature [°C]						
	T_{xri}	T_{ero1}	T_{ero2}	T_{ero3}	T_{ero4}	T_{ref}	
1	45.57	12.49	28.13	35.07	25.97	19.81	
2	47.97	28.18	39.54	29.71	15.11	23.13	
3	49.33	28.48	41.85	32.23	18.22	24.35	
Working conditions	Mass flow rate [g/s]						
	m_1	m_2	m_3	m_4	m		
1	4.0008	3.6211	3.2120	3.5812	14.7785		
2	4.9623	4.8538	4.5346	5.2532	19.7977		
3	6.1642	6.0962	5.7446	6.6161	24.7586		
Working conditions	Quality [-]						
	x_{eri1}	x_{eri2}	x_{eri3}	x_{eri4}	x_{xro}		
1	0.2425	0.2874	0.2165	0.2583	0.2582		
2	0.2711	0.3228	0.2053	0.1698	0.2560		
3	0.2457	0.3038	0.1941	0.1409	0.2441		
Working conditions	Heating power [W]						
	Q_1	Q_2	Q_3	Q_4			
1	543.2125	544.3785	546.9406	550.0297			
2	735.1452	725.8335	735.0394	731.3871			
3	909.0704	914.6850	924.0732	915.4345			

Table 10 Experiment results with uniform heat load under three working conditions at vertical downward orientation

Working conditions	Pressure [kPa]						
	P_{xri}	P_{dri}	P_{ero1}	P_{ero2}	P_{ero3}	P_{ero4}	P_{ero}
1	1447.24	525.44	458.58	451.00	457.57	472.17	388.66
2	1456.54	596.26	505.16	488.75	505.14	503.44	388.07
3	1445.99	693.82	586.13	565.16	565.29	574.42	385.50
Working conditions	Temperature [°C]						
	T_{xri}	T_{ero1}	T_{ero2}	T_{ero3}	T_{ero4}	T_{ero}	T_{ref}
1	42.60836	21.79148	42.6695	17.56058	13.86535	23.18835	28.57893
2	45.44206	20.22119	51.89106	16.84137	16.0066	30.37674	30.73758
3	47.03176	22.07323	40.502	35.22524	22.68143	30.74851	31.32194
Working conditions	Mass flow rate [g/s]						
	m_1	m_2	m_3	m_4	m		
1	3.6401	3.5723	3.5974	4.0254	15.4571		
2	4.9509	4.7043	4.9510	4.9630	19.9572		
3	6.5522	6.2179	6.0652	6.2763	25.4485		
Working conditions	Quality [-]						
	x_{eri1}	x_{eri2}	x_{eri3}	x_{eri4}	x_{xro}		
1	0.2220	0.3139	0.1909	0.0274	0.1980		
2	0.1754	0.3026	0.1573	0.1540	0.1941		
3	0.1700	0.2344	0.1848	0.1426	0.1723		
Working conditions	Heating power [W]						
	Q_1	Q_2	Q_3	Q_4			
1	563.1715	563.2765	563.716	564.4701			
2	778.0355	776.2041	778.6064	777.9824			
3	995.5292	995.6949	995.2789	996.2898			

Table 11 Experiment results with uniform mass flow rate under three working conditions at vertical downward orientation

Working conditions	Pressure [kPa]						
	P_{xri}	P_{dri}	P_{ero1}	P_{ero2}	P_{ero3}	P_{ero4}	P_{ero}
1	1447.24	525.44	458.58	451.00	457.57	472.17	388.66
2	1456.54	596.26	505.16	488.75	505.14	503.44	388.07
3	1445.99	693.82	586.13	565.16	565.29	574.42	385.50
Working conditions	Temperature [°C]						
	T_{xri}	T_{ero1}	T_{ero2}	T_{ero3}	T_{ero4}	T_{ero}	T_{ref}
1	42.61	26.48	47.94	23.50	13.07	23.19	28.58
2	45.44	21.42	50.43	18.80	16.52	30.38	30.74
3	47.03	21.03	39.31	33.36	21.93	30.75	31.32
Working conditions	Mass flow rate [g/s]						
	m_1	m_2	m_3	m_4	m		
1	3.6401	3.5723	3.5974	4.0254	15.4571		
2	4.9509	4.7043	4.9510	4.9630	19.9572		
3	6.5522	6.2179	6.0652	6.2763	25.4485		
Working conditions	Quality [-]						
	x_{eri1}	x_{eri2}	x_{eri3}	x_{eri4}	x_{xro}		
1	0.2220	0.3139	0.1909	0.0274	0.1980		
2	0.1754	0.3026	0.1573	0.1540	0.1941		
3	0.1700	0.2344	0.1848	0.1426	0.1723		
Working conditions	Heating power [W]						
	Q_1	Q_2	Q_3	Q_4			
1	578.2150	579.2646	583.6601	591.2009			
2	782.8550	764.5410	788.5642	782.3240			
3	986.7918	988.4494	984.2890	994.3979			